ESA Technical Note / Final Report (January 2020):

CCN #2: Support to MIPAS level 2 processor verification and validation - Phase F

Report to MS6_2: L1v8/L2v8 FM comparison for GL1-GL3

Long-term validation of MIPAS ESA operational products using MIPAS-B measurements

Gerald Wetzel, Michael Höpfner, and Hermann Oelhaf

Karlsruhe Institute of Technology (KIT), Institute of Meteorology and Climate Research (IMK), Karlsruhe, Germany

Table of contents

1 Introduction

The detection of stratospheric trace gases plays a dominant role in a changing climate. Satellite measurements are essential for monitoring the distribution and trend of these species on a global scale. ESA's Environmental Satellite (ENVISAT) operated ten years between 2002 and 2012. The Michelson Interferometer for Passive Atmospheric Sounding (MIPAS; Fischer et al., 2008) was one of three chemistry instruments aboard ENVISAT. The validation of such instruments with the goal of the assessment of the measurement accuracy is an essential task. Stratospheric balloon measurements are particularly suitable to reach this goal since these instruments are able to sound the atmosphere with high vertical resolution. The main logistical issue that the satellite- and the validating balloon instruments observe the same air masses has to be carefully taken into account when performing balloon campaigns. Two principal comparison methods are common: (1) direct matches where the balloon instrument measures at the same time and location where the satellite observation takes place and (2) trajectory matches where forward and backward trajectories are calculated from the balloon measurement geolocation to search for appropriate satellite overpasses. Several flights with the balloon version of MIPAS (Friedl-Vallon et al., 2004) were carried out during the operational time of ENVISAT. In the following sections, validation activities, data analysis and validation results are described in detail.

2 Instruments and data analysis

2.1 MIPAS-E operations and data version

The limb-viewing Fourier transform spectrometer MIPAS on ENVISAT (MIPAS-E) has been designed to operate in the mid-infrared spectral region covering five spectral bands between 685 and 2410 cm^{-1} with an unapodized full spectral resolution of 0.025 cm^{-1} (Fischer et al., 2008). The vertical instantaneous field of view (IFOV) was about 3 km. ENVISAT was launched into its sun-synchronous orbit by ESA on 1 March 2002 with 14.3 orbits/day and an Equator crossing time of 10:00 LT (descending node). After the commissioning phase, MIPAS was run predominantly in its nominal measurement mode with full spectral resolution (called FR mode) from July 2002 until the end of March 2004. During each orbit approximately 72 limb scans covering tangent altitudes between 8 and 68 km were recorded (in steps of 3 km below 45 km) in the FR mode. The majority of validation studies based on correlative measurements published so far were addressing MIPAS data recorded during this first time period. These measurements were originally reprocessed by the ESA Instrument Processing Facilities (IPF) V4.1 and V4.2, based on the Optimized Retrieval Model (ORM) code described in Ridolfi et al. (2000) and in Raspollini et al. (2006), and covered the parameters p, T, and the six constituents H_2O, O_3, CH_4, N_2O, HNO_3, and NO_2. The validation studies addressed these parameters and constituents: p, T (Ridolfi et al., 2007); O_3 (Cortesi et al., 2007); HNO_3 (Wang et al., 2007); NO_2 (Wetzel et al., 2007); N_2O and CH_4 (Payan et al. 2009); H_2O (Wetzel et al., 2013a).

After an increasing frequency of problems with the interferometer drive system in late 2003 and beginning of 2004 and upon subsequent detailed investigations, it was decided to suspend the nominal operations from March 2004 onwards for detailed investigations. From January 2005 onwards, the instrument was back to operation but at truncated maximum optical path difference (while maintaining the interferogram scan speed) and hence reduced spectral resolution (41% of nominal) for the benefit of an equivalent improvement in the vertical and horizontal (along-track) sampling. The duty cycle of this so-called optimized resolution (OR) mode (optimized in terms of a trade-off between spectral and spatial resolution considering

instrument operation safety aspects) could be steadily increased from 30% in January 2005 to 100% from December 2007 on. MIPAS was successfully operated with this full duty cycle in the OR mode until 8 April 2012, when an ENVISAT anomaly occurred resulting into the loss of communication between ground and satellite and the end of MIPAS observations (ESA, 2012). Details of the characteristics of the two MIPAS mission phases (FR and OR modes) in terms of instrument settings and atmospheric sampling are described in Raspollini et al. (2013).

The coarser spectral but finer spatial sampling of MIPAS since 2005 along with the need for near real time analysis demanded adaptations in the calibration scheme and the processing codes. This was realized in ESA Level 2 processor version 6 and explained by Raspollini et al. (2013), which also give the diagnostics of the products including the error budgets as estimated by Dudhia et al. (2002). The whole MIPAS data set covering almost 10 years of observations was re-processed with v6, v7, and v8. In addition, the number of retrieved constituents was extended to $ClONO_2$, N_2O_5, CFC-11, and CFC-12 (v6). ESA version 7 data (released in 2015) also includes the species HCN, HCFC-22, CF_4, COF_2, and CCl_4. The ESA L1v8/L2v8 DDS diagnostic data set version was released in June 1018 followed by the L1v8/L2v8 FM full mission data in June 2019. The new v8 data release comprises the additional molecules C_2H_2, C_2H_6, $COCl_2$, OCS, CH_3Cl, and HDO. All molecules except HDO have been validated by the MIPAS balloon instrument. Concerning the species C_2H_6, $COCl_2$, and CH_3Cl an updated v8 data set with a new quality flag filtering released in January 2020 was used for the intercomparison of both MIPAS instruments.

2.2 MIPAS-B data set

The balloon-borne limb-emission sounder MIPAS-B was a precursor of the MIPAS satellite instrument (see Friedl-Vallon et al., 2004, and references therein). Hence, a number of specifications like spectral resolution and spectral coverage are similar. However, for essential parameters the MIPAS-B performance is superior, mainly NESR (Noise Equivalent Spectral Radiance) and line of sight stabilization which is based on an inertial navigation system supplemented with an additional star reference system which leads to an after all knowledge of the tangent altitude in the order of 90 m (3σ). The MIPAS-B NESR is further improved by averaging multiple spectra recorded at the same elevation angle. The general data processing from interferograms to calibrated spectra including instrument characterization is described in Friedl-Vallon et al. (2004) and references therein.

MIPAS-B measurements were done typically on a 1.5 km vertical tangent altitude grid. Retrieval calculations of temperature and atmospheric trace species were performed at a 1 km grid up to float altitude (and a coarser grid above this altitude level) with a least squares fitting algorithm using analytical derivative spectra calculated by the Karlsruhe Optimized and Precise Radiative transfer Algorithm (KOPRA; Stiller et al., 2002; Höpfner et al., 2002). To avoid retrieval instabilities due to oversampling of vertical grid points, a regularization approach according to the method described by Tikhonov (1963) and Phillips (1962) constraining with respect to a first derivative a priori profile was adopted. The resulting vertical resolution is typically between 2 and 5 km for the analysed atmospheric parameters and is therefore comparable or slightly better than the vertical resolution of the MIPAS satellite instrument. Table 1 gives an overview of the spectral windows used for the MIPAS-B target parameter retrievals. Different spectral microwindows within mostly the same molecular bands were used for the MIPAS-E data analysis (Raspollini et al., 2013). Spectroscopic parameters for the calculation of the infrared emission spectra originate from the high-resolution transmission (HITRAN) molecular absorption database (Rothman et al., 2009) and a MIPAS dedicated

spectroscopic database (Raspollini et al., 2013). For heavy molecules like CFC-11, CFC-12, HCFC-22, CCl_4, and CF_4, new and improved infrared absorption cross sections (Harrison, 2015; Harrison, 2016; Harrison et al., 2017) were used for the calculation of radiative transfer. The MIPAS-B error budget includes random noise as well as covariance effects of the fitted parameters, temperature errors, pointing inaccuracies, errors of non-simultaneously fitted interfering species, and spectroscopic data errors (1 σ). For further details on the MIPAS-B data analysis and error estimation, see Wetzel et al. (2012, 2015) and references therein.

2.3 Validation approach

A number of MIPAS balloon flights have been carried out as part of the validation programme of the chemistry instruments aboard ENVISAT. Most of the MIPAS-B data used here, however, were obtained during flights that were done in the framework of various scientific projects. MIPAS-B has a sophisticated pointing system so that the full freedom of a balloon-borne limb emission sounder in terms of observation time, viewing direction and sampling strategy could be used to get the best possible coincidence in time and space with the satellite overpass even during balloon flights that were not primarily dedicated to satellite validation. If compliant with the scientific goal of the mission and the weather conditions, the strategy was to launch the balloon in due time before an ENVISAT overpass and to optimize the azimuthal viewing direction and the vertical sampling at the time of the overpass. Except two flights, a coincidence in space and time between both sensors could be achieved such that vertical profiles of both instruments can be directly compared. An overview of the MIPAS balloon flights used in this study is given in Table 2.

To enhance the statistics of profile comparisons diabatic 2-day forward and backward trajectories were calculated by the Free University of Berlin using a trajectory model (Naujokat and Grunow, 2003; Grunow, 2009). The trajectories are based on European Centre for Medium-Range Weather Forecasts (ECMWF) 1.25°x1.25° analyses and start at different altitudes at the geolocation of the balloon observation to search for a coincidence with the satellite measurement along the trajectory path within a match radius of 1 h and 500 km. Temperature and volume mixing ratio (VMR) of the satellite match have been interpolated to the trajectory match altitude such that these values can be directly compared to the MIPAS-B data at the trajectory start point altitude. Altitude differences between the trajectory start- and match point have to be taken into account in the case of temperature by means of an adiabatic correction.

The primary vertical coordinate of MIPAS-E is pressure whereas for MIPAS-B it is altitude. For all comparisons shown in this study, vertical profiles refer to the MIPAS-B pressure-altitude grid. Differences between measured quantities of MIPAS-E and the validation instrument MIPAS-B are expressed in absolute and relative units. The mean difference Δx_{mean} for N profile pairs of compared observations is given as:

$$\Delta x_{mean} = \frac{1}{N} \sum_{n=1}^{N} (x_{E,n} - x_{B,n}) , \tag{1}$$

where x_E and x_B are data values of MIPAS-E and MIPAS-B at one altitude level. The mean relative difference $\Delta x_{mean,rel}$ of a number of profile pairs is calculated by dividing the mean absolute difference by the mean profile value of the reference instrument MIPAS-B:

$$\Delta x_{mean,rel} = \frac{\Delta x_{mean}}{\frac{1}{N}\sum_{n=1}^{N} x_{B,n}} \cdot 100\% \quad . \tag{2}$$

Differences are displayed together with the combined errors σ_{comb} of both instruments, which are defined as:

$$\sigma_{comb} = \sqrt{\sigma_E^2 + \sigma_B^2} \ , \tag{3}$$

where σ_E and σ_B are the precision, systematic or total errors of MIPAS-E and MIPAS-B, respectively.

Precision errors characterize the reproducibility of a measurement and correspond, in general, to random noise errors. Systematic errors of the operational processor used for MIPAS-E data analysis have been assessed in corresponding studies (Dudhia et al. (2002); Raspollini et al., 2013). The latest error version was released in September 2019. The uncertainty of the calculated mean difference (standard error of the mean, SEM) is given by $\sigma/N^{0.5}$ where σ is the standard deviation (SD). A bias between both instruments is considered significant if the SEM is smaller than the bias itself. The comparison between the VMR difference and the combined systematic error (for statistical comparisons) or total error (for single comparisons) is appropriate to identify unexplained biases in the MIPAS-E measurements when they exceed these combined error limits. Since the vertical resolution of the atmospheric parameter profiles of both instruments is of comparable magnitude, a smoothing by averaging kernels has not been applied to the observed profiles. The method described above was performed for each individual balloon flight comparison. A mean difference (with mean statistical parameters) for all flights was calculated by weighting the mean result of each individual flight equally.

Photochemically reactive gases like NO_2 and N_2O_5, and, to a lesser extent, $ClONO_2$ (mainly in the tropics) undergo a diurnal variation with changing solar zenith angle (SZA). For these gases, a photochemical correction taking into account differences in the SZA between the measurements of both sensors has been applied. The most pronounced temporal variation exhibits the molecule NO_2. The partitioning of NO, NO_2, and N_2O_5 within the NO_y family depends strongly on SZA due to the rapid photolysis of NO_2 and the slower photolysis of N_2O_5. A 1-dimensional model (Bracher et al., 2005) was constrained with NO_y species measured by MIPAS-B and initialized with the output of a global 2-dimensional model (Sinnhuber et al., 2003) to calculate SZA correction factors for the MIPAS-E data.

3 Intercomparison results

In the following subsections, we discuss the validation for all quantities delivered operationally by the L1v8/L2v8 FM processor based on collocated MIPAS-B observations (validation results of previously released data versions are discussed elsewhere, see Wetzel et al., 2016, 2017, 2018). Only MIPAS satellite data that have passed the a posteriori quality check (mainly retrieval convergence and size of maximum error) were used for the intercomparison. The results of the statistical analysis of all compared vertical profiles is regarded as evaluation with the highest statistical evidence. Each figure displays the number of collocated data pairs of MIPAS-E, MIPAS-B used (red numbers) and their mean difference (red solid line) including the standard deviation (red dotted lines) and standard error of the mean (SEM, plotted as error

bars). In addition, the combined errors of MIPAS-B and MIPAS-E are shown in terms of precision (blue dotted lines), systematic error (blue dash-dotted lines) and total error (blue dashed lines), both in absolute and relative units (left and right panels, respectively). Trajectory matches are based on diabatic 2-day forward and backward trajectories with a collocation criterion of 1 h and 500 km as described in section 2.

Since the balloon flights were performed between 2002 and 2011, they cover almost the full ENVISAT operational time of 2002 to 2012, i.e. both MIPAS-E mission phases (FR and OR modes) with distinctly different instrument settings. A compilation of all vertical profiles of temperature and 20 species retrieved from MIPAS-B spectra is given in Figure 1. We performed the intercomparison analysis separately not only for different climatological regions but also for the periods 2002-2004 and 2005-2012. The following intercomparison is focused on these two periods when MIPAS-E was operated in the FR and OR mode, respectively. An overview of the intercomparison is given in Table 3.

3.1 Temperature

Apart from its relevance as primary atmospheric state parameter the quality of temperature data is essential in limb sounding since temperature errors propagate in subsequent retrievals of trace constituents. Our study shows that above about 11 km the mean differences between MIPAS-B and MIPAS-E are within ±2 K and within the combined systematic errors although the standard deviations exceed the expected precision (see Figure 2). In the lowermost stratosphere and around the tropopause, MIPAS-E exhibits a positive bias with respect to the balloon instrument in the OR mode and the tropics. In general, temperatures are slightly higher (~0.2 K) in L1v8/L2v8 data compared to v7 data. Differences between both sensors are still comparable to the findings of a comprehensive temperature validation study by Ridolfi et al. (2007) that was addressing the FR mode period only using version 4.61 and 4.62 data.

3.2 H_2O

In view of the debates on long-term trends of water vapour (see e.g. Dessler et al., 2014; Lossow et al., 2018, Khosrawi et al., 2018) we carefully looked at the consistency of the validation results of the MIPAS-E FR phase with respect to the OR phase. Figure 3 presents the intercomparison results. FR and OR mode comparisons show different vertical shapes of the differences between MIPAS-E and MIPAS-B. In the lowermost stratosphere and upper troposphere MIPAS-E significantly overestimates H_2O and exceeds the combined systematic error bars around 15 km in the OR mode. This general behaviour remains also in the statistical analysis of all collocations. In the middle and upper stratosphere, a positive bias of MIPAS-E vs. MIPAS-B (increasing with altitude in the FR period) of 5-20% is visible although the errors stay (except at 37 km) within the predicted error budget. This bias is slightly reduced compared to v7 data due to somewhat (~0.1 ppmv) lower H_2O values in the MIPAS-E retrievals. These findings support the conclusions drawn from a comprehensive validation study of MIPAS-E phase one (FR mode) observations by Wetzel et al. (2013a).

3.3 O_3

Comparisons based on the full statistics over all collocations show an agreement between the satellite and the balloon data within ±10% above 15 km for this mainly stratospheric species (see Figure 4). For most of the stratosphere (17-37 km), the mean relative difference between the data sets is always within ±5%. Furthermore, differences of the combined FR plus OR mode

are within the combined systematic error. Degradation in the quality of the agreement is observed in the lower stratosphere and upper troposphere, with deviations up to about 20% in both observation periods. Generally, the statistical agreement of both data sets is comparable to that reported by Cortesi et al. (2007) for the FR mode phase as deduced from an extensive study using various kinds of correlative data. The present L1v8/L2v8 data version does not exhibit a striking difference compared to the previous v7 one.

3.4 HNO_3

VMR difference profiles for the stratospheric nitrogen reservoir species HNO_3 are presented in Figure 5. MIPAS-E tends to overestimate the HNO_3 abundance when compared to MIPAS-B below about 27 km. This bias is most prominent in the OR mode data between 19 and 26 km around the altitude of the VMR maximum of the HNO_3 profile and somewhat enhanced compared to the v7 data. Biases are typically in the order of 5-20% in relative units and in line with the numbers reported by Wang et al. (2007) referring to the FR period. Standard deviations clearly exceed the expected precision.

3.5 CH_4 and N_2O

These two species are long-lived tracers of similar lifetimes and are therefore correlated to each other. Hence, they are discussed together in this study. Figures 6 and 7 present the results for these molecules based on the statistical trajectory analysis of all collocations available. Both species show a quite similar altitude-dependent behaviour of the mean difference in absolute and relative quantities while standard deviations exceed the expected precision. MIPAS-E tends to overestimate the abundance of both species in the stratosphere below about 35 km by 5-15% (CH_4) and 10-20% (N_2O). A similar positive bias has already been stated in the (FR mode) validation study by Payan et al. (2009). Somewhat larger positive deviations are visible in the Tropics around 30 km. Changes in the VMR differences using the current L1v8/L2v8 data set compared to the VMR differences taking the v7 data are small.

3.6 NO_2

NO_2 exhibits a strong diurnal variation in the stratosphere and is in photochemical equilibrium with NO and N_2O_5 (see, e.g., Brasseur and Solomon, 2005). This needs to be taken into account when comparing MIPAS-E NO_2 data sets. For our study, a photochemical correction considering differences in the SZA between the measurements of both sensors has been applied as described in more detail in section 2. Figure 8 presents the statistical trajectory match analysis. It indicates a positive bias (up to 20%, unexplained above 31 km) of MIPAS-E NO_2 in the FR period that is becoming increasingly significant from lower to higher altitudes. This is in line with the findings of the comprehensive NO_2 validation study (FR mode) reported by Wetzel et al. (2007). In the OR period, the positive bias (above 27 km) between both sensors is smaller (~10%). No striking changes compared to the previous v7 data can be recognized.

3.7 Additional v6 products: N_2O_5, $ClONO_2$, CFC-11, and CFC-12

Starting with processor v6, four additional target species, namely N_2O_5, $ClONO_2$, CFC-11, and CFC-12, have been operationally processed by ESA. A first validation study of these species was carried out by Wetzel et al. (2013b).

N_2O_5 is a temporary reservoir of reactive nitrogen in the stratosphere and exhibits a prominent diurnal variation with maxima just before sunrise and minima just before sunset. The general agreement between MIPAS-E and MIPAS-B (Figure 9) is within ±10% between 24 and 34 km for the mean of all collocations. The behaviour of the complete vertical profile of the mean difference suggests slightly different VMR profiles measured by both instruments (especially in the tropics). Below 24 km and above 34 km mean differences exceed at least partly the systematic errors suggesting a careful use of the MIPAS-E N_2O_5 data for scientific studies in these altitude regimes. No significant bias is visible in the OR mode but a small negative bias is obvious in the FR period. No striking changes compared to v7 data are noticeable.

$ClONO_2$ is a major reservoir of reactive chlorine in the stratosphere and is involved in heterogeneous chemistry in the context of ozone depletion at high latitudes. It undergoes diurnal variations at higher altitudes during periods of stronger illumination, thus it had to be photochemically corrected there. Figure 10 presents the intercomparison results for all collocations. In the altitude region where $ClONO_2$ concentrations are most relevant both data sets are consistent. Differences are within ±10% between 17 and 34 km without a clear bias. Only at the upper and lower altitude edge of the comparisons the mean differences exceed the combined systematic errors. However, standard deviations clearly exceed the expected precision. No striking changes compared to v7 data are visible.

Results for the rather long-lived chlorofluorocarbons CFC-11 (CCl_3F) and CFC-12 (CCl_2F_2) are shown in Figures 11 and 12. In the case of CFC-12 mean differences remain within the combined errors and are within ±5% below 20 km. Above this altitude, a significant positive bias is visible (up to 32 km) and standard deviations exceed the expected precision. Slightly reduced deviations below 16 km compared to v7 data are noticeable. Deviations for the molecule CFC-11 are somewhat larger with up to ±10% below 20 km. An increasing positive bias is obvious above this altitude level. Some enhanced negative deviations below 15 km compared to v7 are obvious.

3.8 Additional v7 products: HCFC-22, CCl_4, CF_4, COF_2, and HCN

Five more species have been operationally processed by the v7 algorithm. To date, an intercomparison study is only available for vertical VMR profiles of the molecule CCl_4 (Valeri et al., 2017). It should be mentioned that these species are generally more difficult to retrieve than the gases described before. This holds also for the MIPAS-B retrieval, although these gases can be measured with higher accuracy (mainly due to lower spectral noise) compared to MIPAS-E. Hence, some unexplained features (exceeding combined systematic errors) in the VMR difference profiles are expected to occur more frequently when comparing these molecules.

HCFC-22 ($CHClF_2$) is a longer-lived hydrochlorofluorocarbon. Since HCFC-22 is often used as an alternative to the highly ozone-depleting CFC-11 and CFC-12, its tropospheric concentration is further increasing (Carpenter et al., 2014). Comparison results are depicted in Figure 13. In the FR mode period differences between both instruments remain within ±10% up to 26 km turning into a significant positive bias above this altitude. In the OR observation period, deviations stay within 10% for altitudes up to 28 km while a significant negative bias is visible in the MIPAS-E data above this altitude level. Standard deviations exceed the expected precision at higher altitudes (mainly OR phase). A slightly reduced negative bias above 28 km compared to previous v7 data is visible.

The tropospheric mixing ratio of the longer-lived source gas CCl_4 is clearly decreasing since the beginning of the 1990s. However, estimated sources and sinks of this molecule are inconsistent with observations of its abundance (Carpenter et al., 2014). A significant negative bias shows up in the MIPAS-E CCl_4 data (full period) above 22 km (see Figure 14), which is at the brink of the combined systematic error limits. A significant positive bias is visible below 21 km during the OR phase. However, differences stay within ±20% up to about 22 km in both observation periods, which is in line with the deviations reported by Valeri et al. (2017). A different shape of deviations compared to v7 data is recognized.

The fluorocarbon CF_4 has an extremely long atmospheric lifetime of more than 50000 years and its atmospheric concentration is linearly increasing (Carpenter et al., 2014). Comparison results are shown in Figure 15. A general agreement between both instruments can be stated between 11 and 37 km (within ±10% in full observation period). In the FR phase, a significant positive bias above 10 km is visible. In contrast, no clear bias is obvious in the OR period where differences stay within ±10% at all altitudes. However, standard deviations exceed the expected precision in the OR phase. Clearly reduced deviations around 26 km compared to v7 are obvious.

The molecule COF_2 is a stratospheric reservoir species for fluorine. The general profile shape (as measured by MIPAS-B) is reproduced by MIPAS-E (see Figure 16). VMR differences stay within ±20% in the stratosphere (deviations in OR mode are larger than in FR mode). No unexplained biases (in terms of combined systematic error bars) are evident. A slightly different shape of deviations compared to v7 data is evident.

HCN is mainly produced by biomass burning and hence considered as an almost unambiguous tracer for biomass burning events (see e.g. Li et al., 2003). Differences are within ±20% below 34 km (see Figure 17). A significant positive bias (more than 20% above 20 km) is evident in the MIPAS-E profiles observed in the FR mode period exceeding the combined systematic error limits above 20 km. This pronounced bias is visible in each comparison of the three MIPAS-B flights in the FR phase. No clear bias can be seen in the OR period. The standard deviation between about 20 and 30 km exceeds the estimated precision in the OR phase. Deviations between both instruments are clearly reduced compared to previous v7 data.

3.9 Additional v8 products: C_2H_2, C_2H_6, $COCl_2$, OCS, and CH_3Cl

Some more target molecules have been operationally processed by the v8 algorithm. To date, an intercomparison study is only available for vertical VMR profiles of the species $COCl_2$ (Valeri et al., 2016). Similar to the additional v7 gases, the emissions of spectral lines of the v8 molecules are also weak compared to the spectral signatures of the standard gases (before v7). Hence, retrievals of these additional species are challenging.

C_2H_2 is mainly produced by biomass burning and, to a lesser extent, by biofuel burning (Singh et al., 1996; Parker et al., 2011; Wiegele et al., 2012). Differences are within ±50% up to 24 km (see Figure 18). A significant negative bias (within -50% difference limit) is evident in the FR mode (except 15-16 km). A significant negative bias below 20 km and above 23 km can be seen in the OR mode (exceeding combined systematic errors and the -50% difference limit). Lower stratospheric altitude regions in MIPAS-E retrievals sometimes show negative VMRs (in Arctic winter). Hence, this species should be carefully used in scientific studies.

C_2H_6 is produced by biomass burning, natural gas losses and fossil fuel production (Rudolph, 1995; Xiao et al., 2008; Glatthor et al., 2009). Differences are within ±25% up to 19 km (see Figure 19). While a significant negative bias is obvious in the FR period (exceeding -50% limit above 13 km), no bias is seen in the MIPAS-E data below 20 km in the OR mode where differences are within a ±20% range. Lower stratospheric altitude regions in MIPAS-E retrievals sometimes show negative VMRs (in the Arctic). Consequently, C_2H_6 profiles should be carefully used in scientific studies.

$COCl_2$ is produced by chemical industries and OH-initiated oxidation of chlorinated hydrocarbons in the troposphere (Kindler et al., 1995; Fu et al., 2007; Valeri et al., 2016). Figure 20 shows that differences are within ±20% up to 27 km in both observation periods such that the general profile shapes (as measured by MIPAS-B) are reproduced by the satellite instrument. A negative bias is evident in the FR and OR period (except 22-27 km), unexplained at high altitudes. Deviations in the Tropics are quite large.

OCS is the most prevalent sulphur-containing species which is transported into the stratosphere where it acts as prerequisite of the stratospheric aerosol layer (Crutzen, 1976; Kremser et al., 2016; Glatthor et al., 2017). Differences are within ±20% up to 24 km in the full measurement period (see Figure 21). A significant positive bias is visible below 22 km and a negative bias above this altitude in the OR period exceeding the ±50% limit and the combined systematic errors above 24 km. The agreement of the VMR profiles of both sensors is better in the FR period. Here, a significant (positive) bias is only visible between 14 and 18 km. In general, differences stay within ±20% for altitudes up to 26 km in the FR phase and ±25% up to 25 km in the OR period. Deviations in the Tropics are quite large.

CH_3Cl is the most abundant halocarbon in the atmosphere and originates from natural and anthropogenic sources (see e.g. Yokouchi et al., 2000). Figure 22 shows that differences stay within ±20% between 13 and 22 km (full observation period). However, the comparison reveals a positive bias above 16 km and a negative bias below this altitude in the FR period. A negative bias within -35% between 19 and 26 km, increasing with altitude, and exceeding the combined systematic errors above 26 km is also visible in the OR period. Large deviations between both instruments occur at midlatitudes and in the Tropics.

4 Conclusions

Vertical profiles of MIPAS balloon flights between 2002 and 2011 covering virtually the whole lifetime of MIPAS on ENVISAT have been used for an intercomparison study of all operational parameters delivered by ESA.

For MIPAS-E (up to v7) stratospheric species (except HCN and CF_4) no striking change in the agreement with MIPAS-B measurements from v7 to L1v8/L2v8 FM data was found. Concerning the molecule HCN, deviations between both instruments were clearly reduced with respect to the v7 data. Furthermore, a scatter of unreasonably large and negative values in the MIPAS-E profiles (Arctic winter, OR phase) in the L1v8/L2v8 DDS (inferring large oscillating VMR differences between both instruments) could be removed in the L1v8/L2v8 FM data set. In the case of CF_4, deviations between the measured profiles of both instruments could be reduced with the present MIPAS-E data version (compared to v7). Altogether, a similar degree of agreement was found between MIPAS-B data and MIPAS-E measured L1v8/L2v8 FM data in the OR and FR operating period. A summary of the main results is given in Table 3.

The comparison of the new v8 species (C_2H_2, C_2H_6, $COCl_2$, OCS, and CH_3Cl) in general exhibits somewhat larger deviations in the retrieved VMR of both instruments (compared to the previous species). Some altitude regions of C_2H_2 and, to a lesser extent, C_2H_6 are characterized by negative MIPAS-E values (mainly in the Arctic winter). While VMR deviations for the gases $COCl_2$ and OCS stay within about 20% in the upper troposphere and lower stratosphere (FR and OR phase), VMR differences for the molecule CH_3Cl exceed the 50% limit in this altitude region in the FR period. Hence, we conclude that the MIPAS-E L1v8/L2v8 FM data of the species C_2H_2, C_2H_6, and CH_3Cl should be used carefully in scientific studies.

5 References

Bracher, A., Sinnhuber, M., Rozanov, A., and Burrows, J. P.: Using a photochemical model for the validation of NO_2 satellite measurements at different solar zenith angles, Atmos. Chem. Phys., 5, 393-408, doi:10.5194/acp-5-393-2005, 2005.

Brasseur, G. and Solomon, S.: Aeronomy of the middle atmosphere (third edition), Atmos. Oceanograph. Sci. Lib., Springer, Dordrecht, The Netherlands, p. 336, 2005.

Carpenter, L. J., and Reimann, S. (Lead Authors), Burkholder, J. B., Clerbaux, C., Hall, B. D., Hossaini, R., Laube, J. C., and Yvon-Lewis, S. A.: Ozone-Depleting Substances (ODSs) and other gases of interest to the Montreal Protocol, Chapter 1 in Scientific Assessment of Ozone Depletion: 2014, Global Ozone Research and Monitoring Project – Report No. 55, World Meteorological Organization, Geneva, Switzerland, 2014.

Cortesi, U., Lambert, J. C., De Clercq, C., Bianchini, G., Blumenstock, T., Bracher, A., Castelli, E., Catoire, V., Chance, K. V., De Mazière, M., Demoulin, P., Godin-Beekmann, S., Jones, N., Jucks, K., Keim, C., Kerzenmacher, T., Kuellmann, H., Kuttippurath, J., Iarlori, M., Liu, G. Y., Liu, Y., McDermid, I. S., Meijer, Y. J., Mencaraglia, F., Mikuteit, S., Oelhaf, H., Piccolo, C., Pirre, M., Raspollini, P., Ravegnani, F., Reburn, W. J., Redaelli, G., Remedios, J. J., Sembhi, H., Smale, D., Steck, T., Taddei, A., Varotsos, C., Vigouroux, C., Waterfall, A., Wetzel, G., and Wood, S.: Geophysical validation of MIPAS-ENVISAT operational ozone data, Atmos. Chem. Phys., 7, 4807-4867, doi:10.5194/acp-7-4807-2007, 2007.

Crutzen, P. J.: The possible importance of CSO for the sulfate layer of the stratosphere, Geophys. Res. Lett., 3, 73–76, 1976.

Dessler, A. E., Schoeberl, M. R., Wang, T., Davis, S. M., Rosenlof, K. H., and Vernier, J.-P.: Variations of stratospheric water vapor over the past three decades, J. Geophys. Res. Atmos., 119, 12588–12598, doi:10.1002/2014JD021712, 2014.

Dudhia, A., Jay, V. L., and Rodgers, C.D.: Microwindow selection for high-spectral-resolution sounders, Appl. Opt. 41, 3665-3673, 2002, (http://eodg.atm.ox.ac.uk/MIPAS/err/).

ESA: ESA declares end of mission for ENVISAT, ESA news 9 May 2012, available at: http://www.esa.int/esaCP/SEM1SXSWT1H_index_0.html, 2012.

Fischer, H., Birk, M., Blom, C., Carli, B., Carlotti, M., von Clarmann, T., Delbouille, L., Dudhia, A., Ehhalt, D., Endemann, M., Flaud, J. M., Gessner, R., Kleinert, A., Koopman, R., Langen, J., López-Puertas, M., Mosner, P., Nett, H., Oelhaf, H., Perron, G., Remedios, J., Ridolfi, M., Stiller, G., and Zander, R.: MIPAS: an instrument for atmospheric and climate research, Atmos. Chem. Phys., 8, 2151-2188, doi:10.5194/acp-8-2151-2008, 2008.

Friedl-Vallon, F., Maucher, G., Kleinert, A., Lengel, A., Keim, C., Oelhaf, H., Fischer, H., Seefeldner, M., and Trieschmann, O.: Design and characterization of the balloon-borne Michelson Interferometer for Passive Atmospheric Sounding (MIPAS-B2), Appl. Opt., 43, 3335-3355, 2004.

Fu, D., Boone, C. D., Bernath, P. F., Walker, K. A., Nassar, R., Manney, G. L., and McLeod, S. D.: Global phosgene observations from the Atmospheric Chemistry Experiment (ACE) mission, Geophys. Res. Lett., 34, L17815, doi:10.1029/2007GL029942, 2007.

Glatthor, N., von Clarmann, T., Stiller, G. P., Funke, B., Koukouli, M. E., Fischer, H., Grabowski, U., Höpfner, M., Kellmann, S., and Linden, A.: Large-scale upper tropospheric pollution observed by MIPAS HCN and C_2H_6 global distributions, Atmos. Chem. Phys., 9, 9619-9634, doi:10.5194/acp-9-9619-2009, 2009.

Glatthor, N., Höpfner, M., Leyser, A., Stiller, G. P., von Clarmann, T., Grabowski, U., Kellmann, S., Linden, A., Sinnhuber, B.-M., Krysztofiak, G., and Walker, K. A.: Global carbonyl sulfide (OCS) measured by MIPAS/Envisat during 2002–2012, Atmos. Chem. Phys., 17, 2631-2652, doi:10.5194/acp-17-2631-2017, 2017.

Grunow, K.: Anwendung von Trajektorien zur ENVISAT-Validierung und zur Untersuchung der Luftmassenherkunft in der Stratosphäre, PhD, Free University Berlin, Berlin, Germany, 2009.

Harrison, J. J.: New and improved infrared absorption cross sections for dichlorodifluoromethane (CFC-12), Atmos. Meas. Tech., 8, 3197-3207, 2015.

Harrison, J. J.: New and improved infrared absorption cross sections for chlorodifluoromethane (HCFC-22), Atmos. Meas. Tech., 9, 2593-2601, 2016.

Harrison, J. J., Boone, C. D., and Bernath, P. F.: New and improved infra-red absorption cross sections and ACE-FTS retrievals of carbon tetrachloride (CCl_4), J. Quant. Spectrosc. Radiat. Transfer, 186, 139-149, 2017.

Höpfner, M., Oelhaf, H., Wetzel, G., Friedl-Vallon, F., Kleinert, A., Lengel, A., Maucher, G., Nordmeyer, H., Glatthor, N., Stiller, G., von Clarmann, T., Fischer, H., Kröger, C., and Deshler, T.: Evidence of scattering of tropospheric radiation by PSCs in mid-IR limb emission spectra: MIPAS-B observations and KOPRA simulations, Geophys. Res. Lett., 29(8), 1278, doi:10.1029/2001GL014443, 2002.

Khosrawi, F., Lossow, S., Stiller, G. P., Rosenlof, K. H., Urban, J., Burrows, J. P., Damadeo, R. P., Eriksson, P., García-Comas, M., Gille, J. C., Kasai, Y., Kiefer, M., Nedoluha, G. E., Noël, S., Raspollini, P., Read, W. G., Rozanov, A., Sioris, C. E., Walker, K. A., and Weigel, K.: The SPARC water vapour assessment II: comparison of stratospheric and lower mesospheric water vapour time series observed from satellites, Atmos. Meas. Tech., 11, 4435-4463, doi:10.5194/amt-11-4435-2018, 2018.

Kindler, T. P., Chameides, W. L., Wine, P. H., Cunnold, D. M., Alyea, F. N., and Franklin, J. A.: The fate of atmospheric phosgene and the stratospheric chlorine loadings of its parent compounds: CCl_4, C_2Cl_4, C_2HCl_3, CH_3CCl_3, and $CHCl_3$, J. Geophys. Res.-Atmos., 100, 1235–1251, doi:10.1029/94JD02518, 1995.

Kremser, S., Thomason, L. W., von Hobe, M., Hermann, M., Deshler, T., Timmreck, C., Toohey, M., Stenke, A., Schwarz, J. P., Weigel, R., Fueglistaler, S., Prata, F. J., Vernier, J.-P., Schlager, H., Barnes, J. E., Antuña-Marrero, J.-C., Fairlie, D., Palm, M., Mahieu, E., Notholt, J., Rex, M., Bingen, C., Vanhellemont, F., Bourassa, A., Plane, J. M. C., Klocke, D., Carn, S. A., Clarisse, L., Trickl, T., Neely, R., James, A. D., Rieger, L., Wilson, J. C.,

and Meland, B.: Stratospheric aerosol - Observations, processes, and impact on climate, Rev. Geophys., 54, 278–335, doi:10.1002/2015RG000511, 2016.

Li, Q., Jacob, D. J., Yantosca, R. M., Heald, C. L., Singh, H. B., Koike, M., Zhao, Y., Sachse, G. W., and Streets, D. G.: A global three-dimensional model analysis of the atmospheric budgets of HCN and CH_3CN: Constraints from aircraft and ground measurements, J. Geophys. Res., 108(D21), 8827, doi:10.1029/2002JD003075, 2003.

Lossow, S., Hurst, D. F., Rosenlof, K. H., Stiller, G. P., von Clarmann, T., Brinkop, S., Dameris, M., Jöckel, P., Kinnison, D. E., Plieninger, J., Plummer, D. A., Ploeger, F., Read, W. G., Remsberg, E. E., Russell, J. M., and Tao, M.: Trend differences in lower stratospheric water vapour between Boulder and the zonal mean and their role in understanding fundamental observational discrepancies, Atmos. Chem. Phys., 18, 8331-8351, doi:10.5194/acp-18-8331-2018, 2018.

Naujokat, B. and Grunow, K.: The stratospheric arctic winter 2002/03: Balloon flight planning by trajectory calculations, 16th Esa Symposium on European Rocket and Balloon Programmes and Related Research, Proceedings, 530, 421–425, 2003.

Parker, R. J., Remedios, J. J., Moore, D. P., and Kanawade, V. P.: Acetylene C_2H_2 retrievals from MIPAS data and regions of enhanced upper tropospheric concentrations in August 2003, Atmos. Chem. Phys., 11, 10243-10257, doi:10.5194/acp-11-10243-2011, 2011.

Payan, S., Camy-Peyret, C., Oelhaf, H., Wetzel, G., Maucher, G., Keim, C., Pirre, M., Huret, N., Engel, A., Volk, M. C., Kuellmann, H., Kuttippurath, J., Cortesi, U., Bianchini, G., Mencaraglia, F., Raspollini, P., Redaelli, G., Vigouroux, C., De Mazière, M., Mikuteit, S., Blumenstock, T., Velazco, V., Notholt, J., Mahieu, E., Duchatelet, P., Smale, D., Wood, S., Jones, N., Piccolo, C., Payne, V., Bracher, A., Glatthor, N., Stiller, G., Grunow, K., Jeseck, P., Te, Y., and Butz, A.: Validation of version-4.61 methane and nitrous oxide observed by MIPAS, Atmos. Chem. Phys., 9, 413-442, doi:10.5194/acp-9-413-2009, 2009.

Phillips, D.: A technique for the numerical solution of certain integral equations of the first kind, J. Assoc. Comput. Math., 9, 84–97, 1962.

Raspollini, P., Belotti, C., Burgess, A., Carli, B., Carlotti, M., Ceccherini, S., Dinelli, B. M., Dudhia, A., Flaud, J.-M., Funke, B., Höpfner, M., López-Puertas, M., Payne, V., Piccolo, C., Remedios, J. J., Ridolfi, M., and Spang, R.: MIPAS level 2 operational analysis, Atmos. Chem. Phys., 6, 5605–5630, doi:10.5194/acp- 6-5605-2006, 2006.

Raspollini, P., Carli, B., Carlotti, M., Ceccherini, S., Dehn, A., Dinelli, B. M., Dudhia, A., Flaud, J.-M., López-Puertas, M., Niro, F., Remedios, J. J., Ridolfi, M., Sembhi, H., Sgheri, L., and von Clarmann, T.: Ten years of MIPAS measurements with ESA Level 2 processor V6 – Part 1: Retrieval algorithm and diagnostics of the products, Atmos. Meas. Tech., 6, 2419-2439, doi:10.5194/amt-6-2419-2013, 2013.

Ridolfi, M., Carli, B., Carlotti, M., von Clarmann, T., Dinelli, B. M., Dudhia, A., Flaud, J.-M., Höpfner, M., Morris, P. E., Raspollini, P., Stiller, G., and Wells, R. J.: Optimized forward model and retrieval scheme for MIPAS near-real-time data processing, Appl. Opt., 39, 1323–1340, 2000.

Ridolfi, M., Blum, U., Carli, B., Catoire, V., Ceccherini, S., Claude, H., De Clercq, C., Fricke, K. H., Friedl-Vallon, F., Iarlori, M., Keckhut, P., Kerridge, B., Lambert, J.-C., Meijer, Y. J., Mona, L., Oelhaf, H., Pappalardo, G., Pirre, M., Rizi, V., Robert, C., Swart, D., von Clarmann, T., Waterfall, A., and Wetzel, G.: Geophysical validation of temperature retrieved by the ESA processor from MIPAS/ENVISAT atmospheric limb-emission measurements, Atmos. Chem. Phys., 7, 4459-4487, doi:10.5194/acp-7-4459-2007, 2007.

Rothman, L. S., Gordon, I. E., Barbe, A., Benner, D. C., Bernath, P. F., Birk, M., Boudon, V., Brown, L. R., Campargue, A., Champion, J.-P., Chance, K., Coudert, L. H., Dana, V., Devi, V. M., Fally, S., Flaud, J.-M., Gamache, R. R., Goldman, A., Jacquemart, D., Kleiner, I., Lacome, N., Lafferty, W. J., Mandin, J.-Y., Massie, S. T., Mikhailenko, S. N., Miller, C. E., Moazzen-Ahmadi, N., Naumenko, O. V., Nikitin, A. V., Orphal, J., Perevalov, V. I., Perrin, A., Predoi-Cross, A., Rinsland, C. P., Rotger, M., Šimečková, M., Smith, M. A. H., Sung, K., Tashkun, S. A., Tennyson, J., Toth, R. A., Vandaele, A. C., and Vander Auwera, J.: The HITRAN 2008 molecular spectroscopic database, J. Quant. Spectrosc. Radiat. Transfer, 110, 533–572, doi:10.1016/j.jqsrt.2009.02.013, 2009.

Rudolph, J.: The tropospheric distribution and budget of ethane, J. Geophys. Res., 100(D6), 11369–11381, 1995.

Singh, H. B., Herlth, D., Kolyer, R., Chatfield, R., Viezee,W., Salas, L. J., Chen, Y., Bradshaw, J. D., Sandholm, S. T., Talbot, R., Gregory, G. L., Anderson, B., Sachse, G. W., Browell, E., Bachmeier, A. S., Blake, D. R., Heikes, B., Jacob, D., and Fuelberg, H. E.: Impact of biomass burning emissions on the composition of the South Atlantic troposphere: Reactive nitrogen and ozone, J. Geophys. Res., 101, 24203–24219, 1996.

Sinnhuber M., Burrows, J. P., Chipperfield, M. P., Jackman, C. H., Kallenrode, M.-B., Künzi, K., and Quack, M.: A model study of the impact of magnetic field structure on atmospheric composition during solar proton events, Geophys. Res. Lett., 30, 1818, 2003.

Stiller, G. P., von Clarmann, T., Funke, B., Glatthor, N., Hase, F., Höpfner, M., and Linden, A.: Sensitivity of trace gas abundances retrievals from infrared limb emission spectra to simplifying approximations in radiative transfer modeling, J. Quant. Spectrosc. Radiat. Transfer, 72(3), 249-280, 2002.

Tikhonov, A.: On the solution of incorrectly stated problems and a method of regularization, Dokl. Acad. Nauk SSSR, 151, 501–504, 1963.

Valeri, M., Carlotti, M., Flaud, J.-M., Raspollini, P., Ridolfi, M., and Dinelli, B. M.: Phosgene in the UTLS: seasonal and latitudinal variations from MIPAS observations, Atmos. Meas. Tech., 9, 4655-4663, doi:10.5194/amt-9-4655-2016, 2016.

Valeri, M., Barbara, F., Boone, C., Ceccherini, S., Gai, M., Maucher, G., Raspollini, P., Ridolfi, M., Sgheri, L., Wetzel, G., and Zoppetti, N.: CCl_4 distribution derived from MIPAS ESA v7 data: intercomparisons, trend, and lifetime estimation, Atmos. Chem. Phys., 17, 10143-10162, doi:10.5194/acp-17-10143-2017, 2017.

Wang, D. Y., Höpfner, M., Blom, C. E., Ward, W. E., Fischer, H., Blumenstock, T., Hase, F., Keim, C., Liu, G. Y., Mikuteit, S., Oelhaf, H., Wetzel, G., Cortesi, U., Mencaraglia, F.,

Bianchini, G., Redaelli, G., Pirre, M., Catoire, V., Huret, N., Vigouroux, C., De Mazière, M., Mahieu, E., Demoulin, P., Wood, S., Smale, D., Jones, N., Nakajima, H., Sugita, T., Urban, J., Murtagh, D., Boone, C. D., Bernath, P. F., Walker, K. A., Kuttippurath, J., Kleinböhl, A., Toon, G., and Piccolo, C.: Validation of MIPAS HNO_3 operational data, Atmos. Chem. Phys., 7, 4905-4934, doi:10.5194/acp-7-4905-2007, 2007.

Wetzel, G., Bracher, A., Funke, B., Goutail, F., Hendrick, F., Lambert, J.-C., Mikuteit, S., Piccolo, C., Pirre, M., Bazureau, A., Belotti, C., Blumenstock, T., De Mazière, M., Fischer, H., Huret, N., Ionov, D., López-Puertas, M., Maucher, G., Oelhaf, H., Pommereau, J.-P., Ruhnke, R., Sinnhuber, M., Stiller, G., Van Roozendael, M., and Zhang, G.: Validation of MIPAS-ENVISAT NO_2 operational data, Atmos. Chem. Phys., 7, 3261-3284, doi:10.5194/acp-7-3261-2007, 2007.

Wetzel, G., Oelhaf, H., Kirner, O., Friedl-Vallon, F., Ruhnke, R., Ebersoldt, A., Kleinert, A., Maucher, G., Nordmeyer, H., and Orphal, J.: Diurnal variations of reactive chlorine and nitrogen oxides observed by MIPAS-B inside the January 2010 Arctic vortex, Atmos. Chem. Phys., 12, 6581-6592, doi:10.5194/acp-12-6581-2012, 2012.

Wetzel, G., Oelhaf, H., Berthet, G., Bracher, A., Cornacchia, C., Feist, D. G., Fischer, H., Fix, A., Iarlori, M., Kleinert, A., Lengel, A., Milz, M., Mona, L., Müller, S. C., Ovarlez, J., Pappalardo, G., Piccolo, C., Raspollini, P., Renard, J.-B., Rizi, V., Rohs, S., Schiller, C., Stiller, G., Weber, M., and Zhang, G.: Validation of MIPAS-ENVISAT H_2O operational data collected between July 2002 and March 2004, Atmos. Chem. Phys., 13, 5791-5811, doi:10.5194/acp-13-5791-2013, 2013a.

Wetzel, G., Oelhaf, H., Friedl-Vallon, F., Kleinert, A., Maucher, G., Nordmeyer, H., and Orphal, J.: Long-term intercomparison of MIPAS additional species $ClONO_2$, N_2O_5, CFC-11, and CFC-12 with MIPAS-B measurements, Annals of Geophysics, 56, Fast Track-1, doi:10.4401/ag-6329, 2013b.

Wetzel, G., Oelhaf, H., Birk, M., de Lange, A., Engel, A., Friedl-Vallon, F., Kirner, O., Kleinert, A., Maucher, G., Nordmeyer, H., Orphal, J., Ruhnke, R., Sinnhuber, B.-M., and Vogt, P.: Partitioning and budget of inorganic and organic chlorine species observed by MIPAS-B and TELIS in the Arctic in March 2011, Atmos. Chem. Phys., 15, 8065-8076, 2015.

Wetzel, G., Höpfner, M., and Oelhaf, H.: Long-term validation of MIPAS ESA operational products using MIPAS-B measurements, Report to MS1 (L1v7/L2v7 FM validation for GL1+GL2) and MS2 (L1v7/L2v7 FM validation for GL2), ESA Technical Note, 2016.

Wetzel, G., Höpfner, M., and Oelhaf, H.: Long-term validation of MIPAS ESA operational products using MIPAS-B measurements, Report to MS4: L1v7/L2v8 DDS (instead of L1v8/L2v7 DDS) validation for T, H_2O, and O_3, ESA Technical Note, 2017.

Wetzel, G., Höpfner, M., and Oelhaf, H.: Long-term validation of MIPAS ESA operational products using MIPAS-B measurements, Report to MS3_2: L1v8/L2v8 DDS comparison for GL1-GL3, ESA Technical Note, 2018.

Wiegele, A., Glatthor, N., Höpfner, M., Grabowski, U., Kellmann, S., Linden, A., Stiller, G., and von Clarmann, T.: Global distributions of C_2H_6, C_2H_2, HCN, and PAN retrieved from

MIPAS reduced spectral resolution measurements, Atmos. Meas. Tech., 5, 723-734, doi:10.5194/amt-5-723-2012, 2012.

Xiao, Y., Logan, J. A., Jacob, D. J., Hudman, R. C., Yantosca, R., and Blake, D. R.: Global budget of ethane and regional constraints on US sources, J. Geophys. Res., 113, D21306, doi:10.1029/2007JD009415, 2008.

Yokouchi, Y., Noijiri, Y., Barrie, L. A., Toom-Sauntry, D., Machida, T., Inuzuka, Y., Akimoto, H., Li, H.-J., Fujinuma, Y., and Aoki, S.: A strong source of methyl chloride to the atmosphere from tropical coastal land, Nature, 403, 295–298, 2000.

6 Tables and Figures

Table 1. Overview of MIPAS-B spectral windows used for the analysis of atmospheric target parameters together with typical precision errors and total errors.

Target parameter	Spectral range (cm^{-1})	Precision error	Total error
Temperature	801.1 – 813.2 941.3 – 956.7	0.2 – 0.3 K	0.5 – 1.0 K
H_2O	808.0 – 825.3 1210.2 – 1244.5 1585.0 – 1615.0	1 – 2 %	8 – 11 %
O_3	763.5 – 824.4 964.9 – 969.0 1140.1 – 1195.6	0.1 – 1 %	8 – 10 %
HNO_3	864.0 – 874.0	0.2 – 2 %	8 – 9 %
CH_4 & N_2O	1161.9 – 1229.8	1 – 3 %	6 – 10 %
NO_2	1585.0 – 1615.0	1 – 3 %	10 – 12 %
N_2O_5	1220.0 – 1270.0	0.4 – 2 %	5 – 7 %
$ClONO_2$	779.7 – 780.7	2 – 3 %	5 – 6 %
CFC-11	840.0 – 860.0	2 – 3 %	5 – 6 %
CFC-12	918.0 – 924.0	2 – 3 %	5 – 6 %
HCFC-22	828.0 – 830.0	3 – 6 %	9 – 12 %
CCl_4	786.0 – 806.0	5 – 10 %	11 – 15 %
CF_4	1274.3 – 1288.0	2 – 6 %	6 – 11 %
COF_2	750.0 – 776.0	1 – 3 %	10 – 12 %
HCN	750.0 – 776.0	4 – 8 %	9 – 12 %
C_2H_2	750.2 – 790.1	5 – 10 %	7 – 12 %
C_2H_6	811.5 – 835.8	8 – 12 %	12 – 15 %
$COCl_2$	838.3 – 860.0	2 – 5 %	20 – 22 %
OCS	842.4 – 876.0	15 – 20 %	18 – 25 %
CH_3Cl	742.5 – 755.0	5 – 15 %	12 – 20 %

Table 2. Overview of MIPAS balloon flights used for intercomparison with MIPAS-E. Distances and times between closest trace gas profile pairs observed by MIPAS-E and the validation instrument refer to an altitude of 20 km (Kiruna) and 30 km (Aire sur l'Adour and Teresina). In addition, 2-day forward/backward trajectories were calculated for each balloon flight to search for further matches with the satellite sensor.

Location	Date	Distance (km)	Time difference (min)
Kiruna, 68 °N	20 Mar 2003	16 / 546	14 / 15
	03 Jul 2003	Trajectories only	
	11 Mar 2009	187 / 248	5 / 6
	24 Jan 2010	109 / 302	5 / 6
	31 Mar 2011	Trajectories only	
Aire sur l'Adour, 44 °N	24 Sep 2002	21 / 588 / 410 / 146	12 /13 / 15 / 16
Teresina, 5 °S	14 Jun 2005	109 / 497 / 184 / 338	228 / 229 / 268 / 269
	06 Jun 2008	224 / 284 / 600 / 194	157 / 158 / 169 / 170

Table 3. Summary of MIPAS-ENVISAT validation results (trajectory comparison to eight MIPAS-B flights). Mentioned atmospheric parameter differences refer to MIPAS-ENVISAT minus the balloon instrument.

Parameter	Comments (L1v8/L2v8 FM)
Temp.	Difference within ±2 K between 12 and 39 km. Slightly **higher temperatures in L1v8/L2v8 data** (~0.2 K) compared to v7 data.
H_2O	Positive bias (5-20%) between 11 and 39 km within combined systematic errors (except OR mode around 15 km). **Bias reduced** (w.r.t. v7 data) due to lower (~0.1 ppmv) MIPAS-E values.
O_3	Disagreement within ±10% for all altitudes above 15 km. No striking difference compared to v7 data.
HNO_3	Significant positive bias (5-20%) below 27 km (most pronounced between 19 and 26 km in the OR mode and somewhat enhanced compared to v7 data).
CH_4 & N_2O	Positive bias for CH_4 (5-15%) and N_2O (10-20%) below 35 km, especially pronounced in the lowermost stratosphere around 15 km. Somewhat larger positive deviations also in the Tropics around 30 km. Only small changes compared to v7 data.
NO_2	Positive bias of up to 20% in FR mode (unexplained above 31 km), smaller positive bias (~10%) in OR mode (above 27 km). No striking changes compared to v7 data.
N_2O_5	Differences within ±10% between 24 and 34 km (no significant bias in OR mode, small negative bias in FR period). No striking changes compared to v7 data.
$ClONO_2$	Differences within ±10% between 17 and 34 km (no significant bias). No striking changes compared to v7 data.
CFC-11	Differences within 10% below 20 km. Positive bias (increasing with altitude) above this altitude level. Some enhanced negative deviations below 15 km compared to v7.
CFC-12	Differences within ±5% for altitudes below 20 km. Significant positive bias above this altitude level up to 32 km. Slightly reduced deviations below 16 km compared to v7.
HCFC-22	Differences within ±10% up to 26 km (FR mode) and 28 km (OR mode). Significant positive bias above 26 km (FR mode) and significant negative bias above 28 km (OR mode). Slightly reduced negative bias above 28 km compared to v7 data.
CCl_4	Differences within ±20% up to about 22 km in both observation periods. Significant negative bias above 22 km (full period). Significant positive bias below 21 km (OR period). Different shape of deviations compared to v7 data.
CF_4	Differences within ±10% between 11 and 37 km (full period). Significant positive bias above 10 km in FR period. No clear bias in OR period. Clearly **reduced deviations around 26 km compared to v7 data.**
COF_2	Differences within ±20% in the stratosphere; no unexplained biases. Slightly different shape of deviations compared to v7 data.
HCN	Differences within ±20% below 34 km. Stratospheric positive bias in FR mode, exceeding combined systematic errors above 20 km (difference > 20%). No clear bias in OR period. Clearly **reduced deviations compared to previous v7 data.**
C_2H_2	Differences within ±50% up to 24 km. Negative bias (within 50%) in FR mode (except 15-16 km), significant negative bias below 20 km and above 23 km in OR mode (exceeding combined systematic errors and the -50% difference limit). Lower stratospheric altitude regions in MIPAS-E retrievals sometimes show **negative VMRs** (in **Arctic winter**).
C_2H_6	Differences within ±25% up to 19 km. Significant negative bias in FR mode (exceeding -50% limit above 13 km), no bias in OR mode below 20 km (differences within ±20%). Lower stratospheric altitude regions in MIPAS-E retrievals sometimes show **negative VMRs** (in the **Arctic**).
$COCl_2$	Differences within ±20% up to 27 km in both periods. Negative bias in FR and OR period (except 22-27 km), unexplained at high altitudes; **quite large deviations in the Tropics.**
OCS	Differences within ±20% up to 24 km in full period. Significant positive bias between 14 and 18 km; difference within ~20% up to 26 km. (FR mode) and ~25% up to 25 km (OR mode). Significant positive bias < 22 km and negative bias > 22 km (OR mode) exceeding ±50% limit and combined systematic errors above 24 km**; quite large deviations in the Tropics.**
CH_3Cl	Differences within ±20% between 13 and 22 km. Positive bias above 16 km (neg. bias below) in FR period. Negative bias within -35% between 19 and 26 km, increasing with altitude, and exceeding the combined systematic errors above 26 km (OR period). **Large deviations at midlatitudes and in the tropics**.

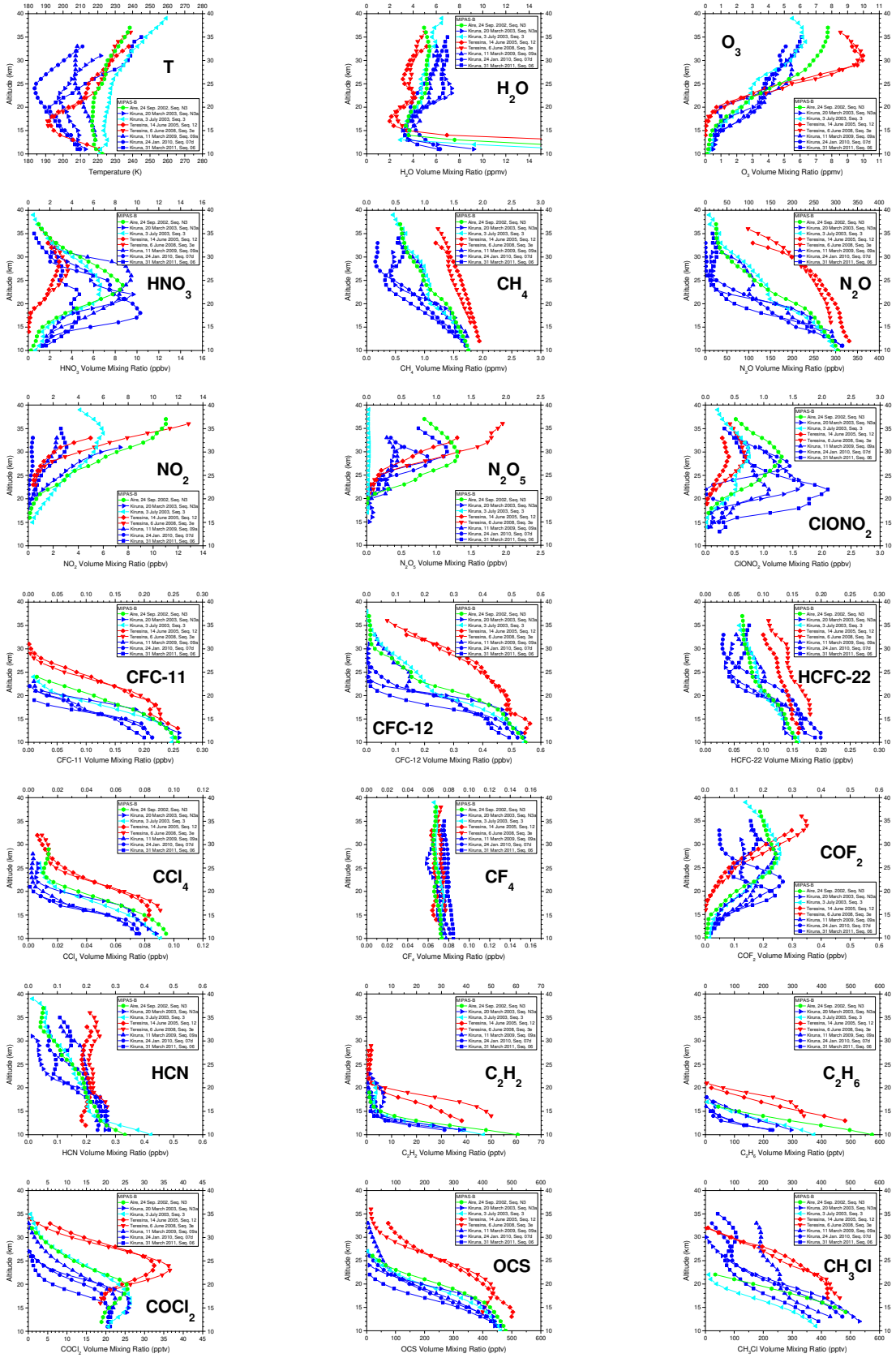

Figure 1. Retrieved vertical profiles of temperature and species of Arctic winter (blue), Arctic summer (cyan), midlatitude (green) and tropical (red) MIPAS-B flights as listed in Table 2.

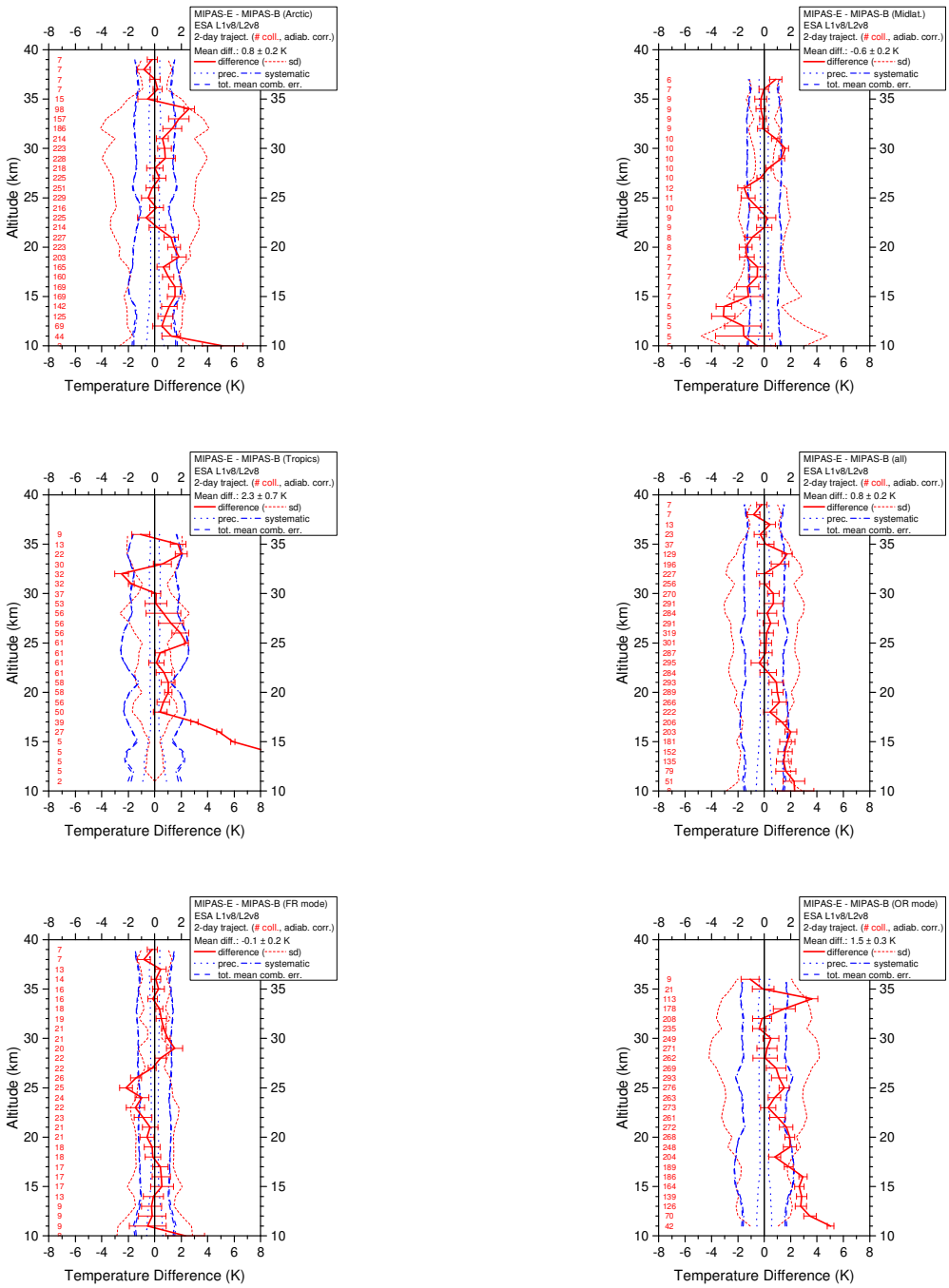

Figure 2. Mean temperature difference (red solid line) of all trajectory match collocations (red numbers) between MIPAS-E and MIPAS-B including standard deviation (red dotted lines) and standard error of the mean (plotted as error bars). Precision (blue dotted lines), systematic (blue dash-dotted lines), and total (blue dashed lines) mean combined errors are shown, too. Top: Arctic (left) and midlatitude (right) collocations; middle: Tropics (left) and all FR plus OR (right) collocations; bottom: FR mode (left) and OR mode (right) collocations. For details, see text.

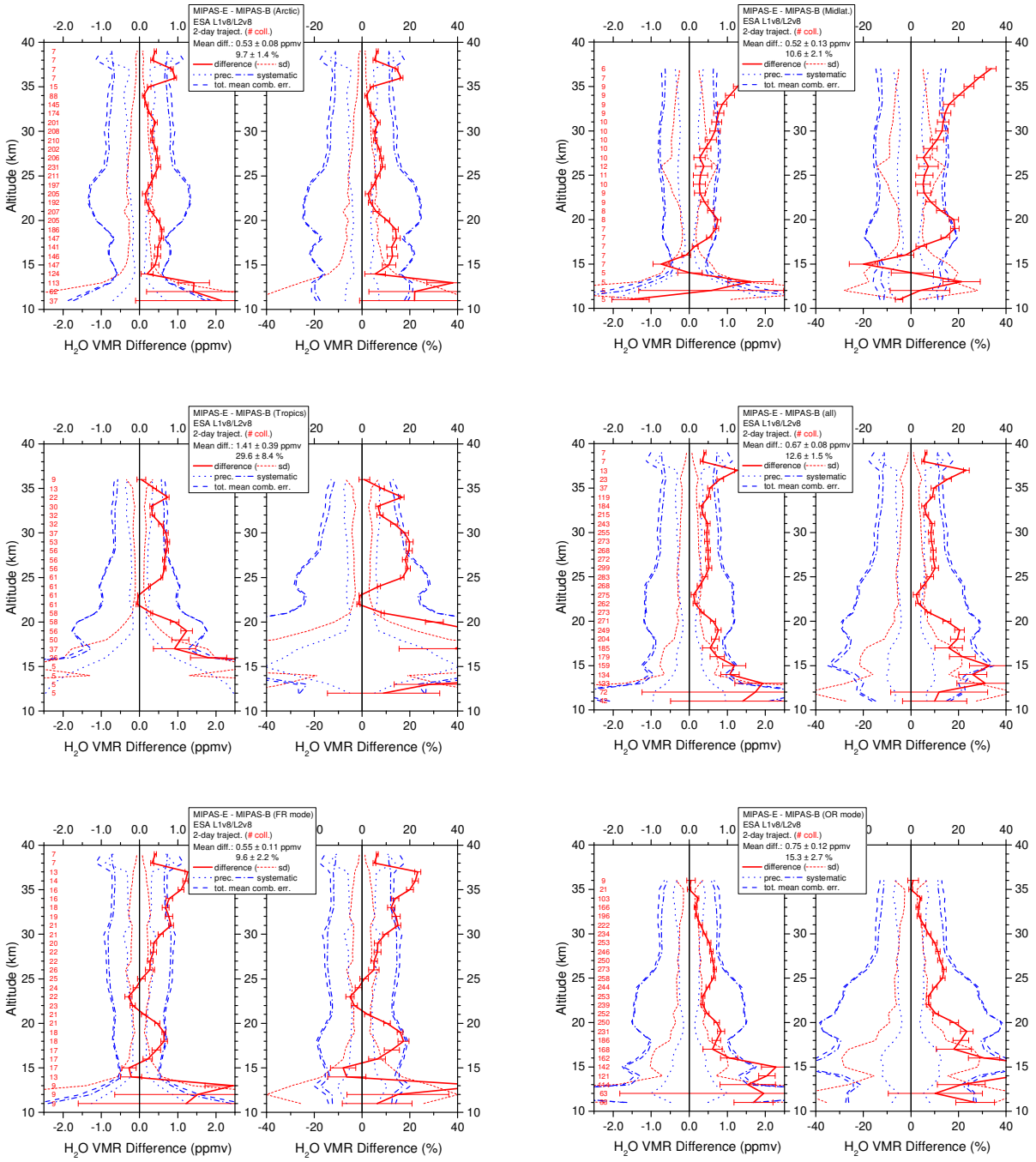

Figure 3. Mean absolute and relative H_2O VMR difference of all trajectory match collocations (red numbers) between MIPAS-E and MIPAS-B (red solid line) including standard deviation (red dotted lines) and standard error of the mean (plotted as error bars). Precision (blue dotted lines), systematic (blue dash-dotted lines), and total (blue dashed lines) mean combined errors are shown, too. Top: Arctic (left) and midlatitude (right) collocations; middle: Tropics (left) and all FR plus OR (right) collocations; bottom: FR mode (left) and OR mode (right) collocations. For details, see text.

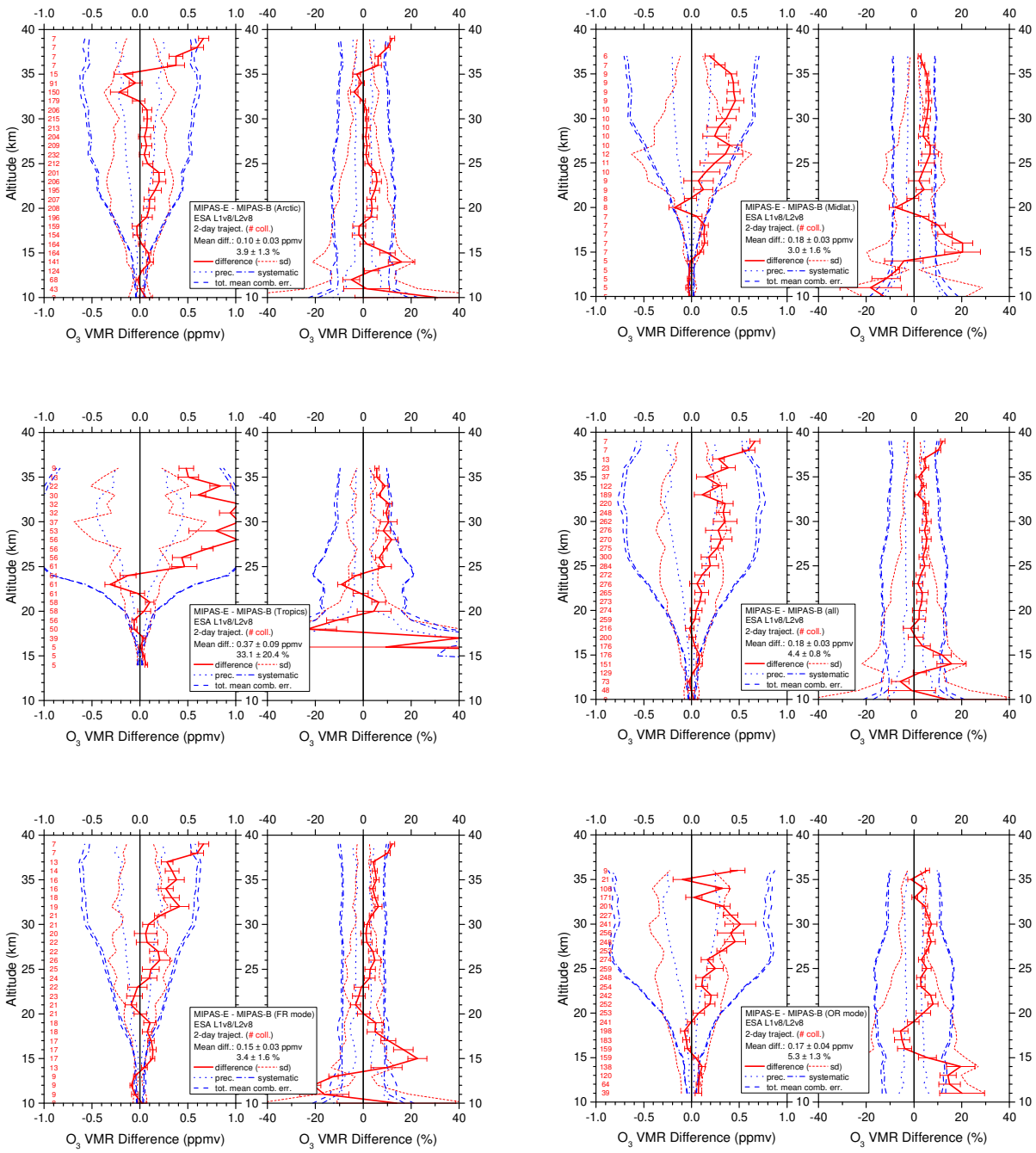

Figure 4. Same as Figure 3 but for O_3.

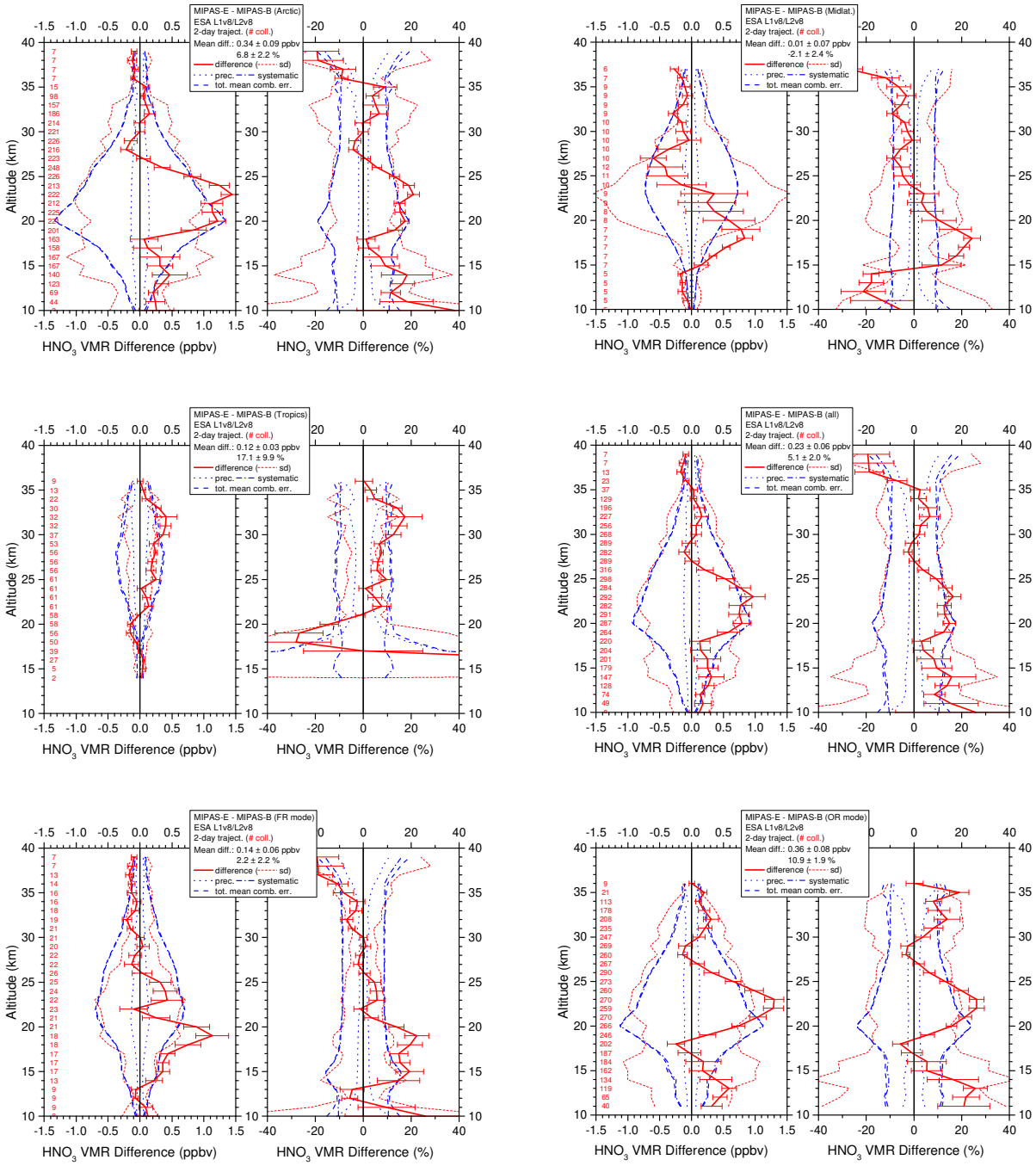

Figure 5. Same as Figure 3 but for HNO_3.

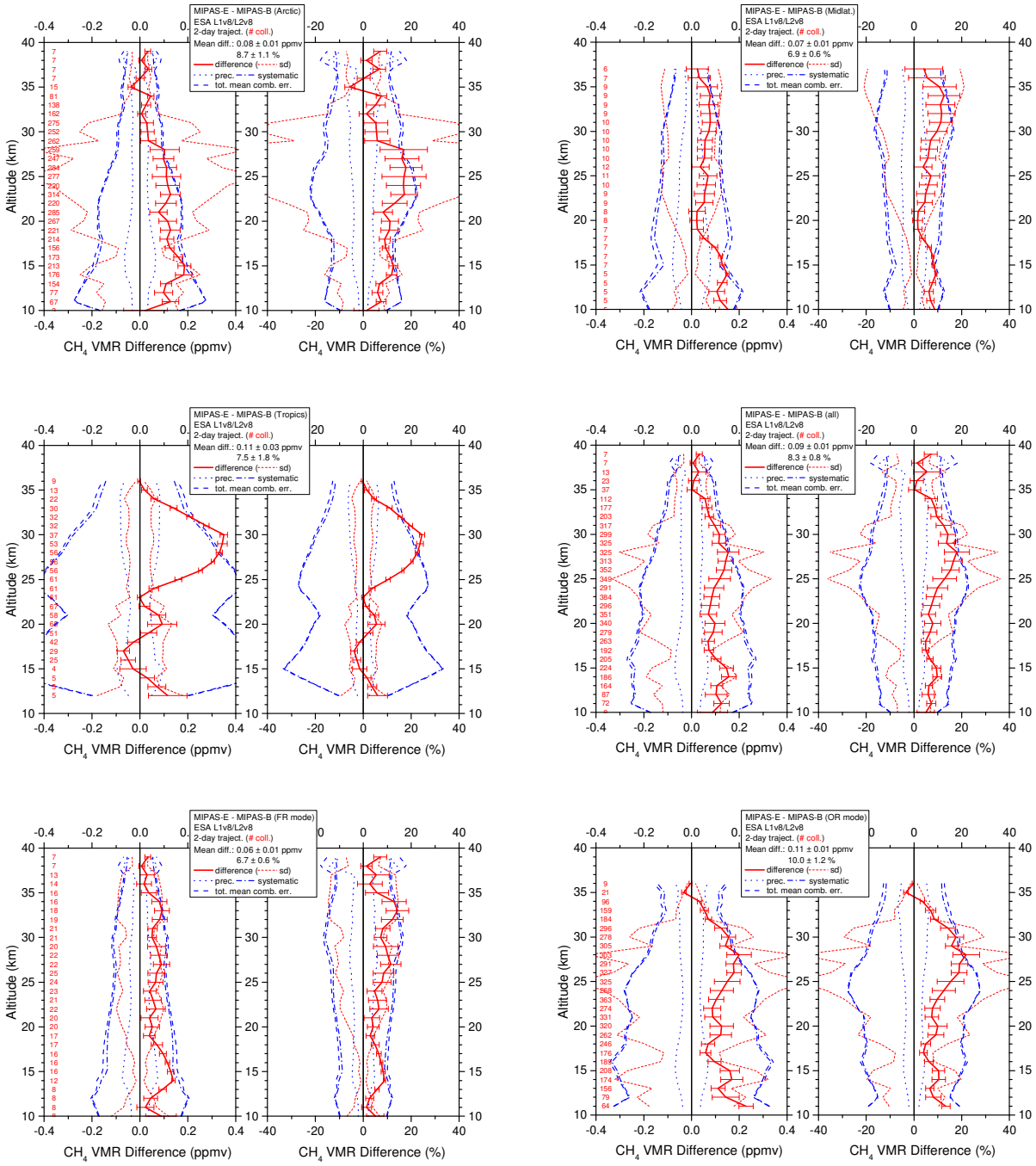

Figure 6. Same as Figure 3 but for CH_4.

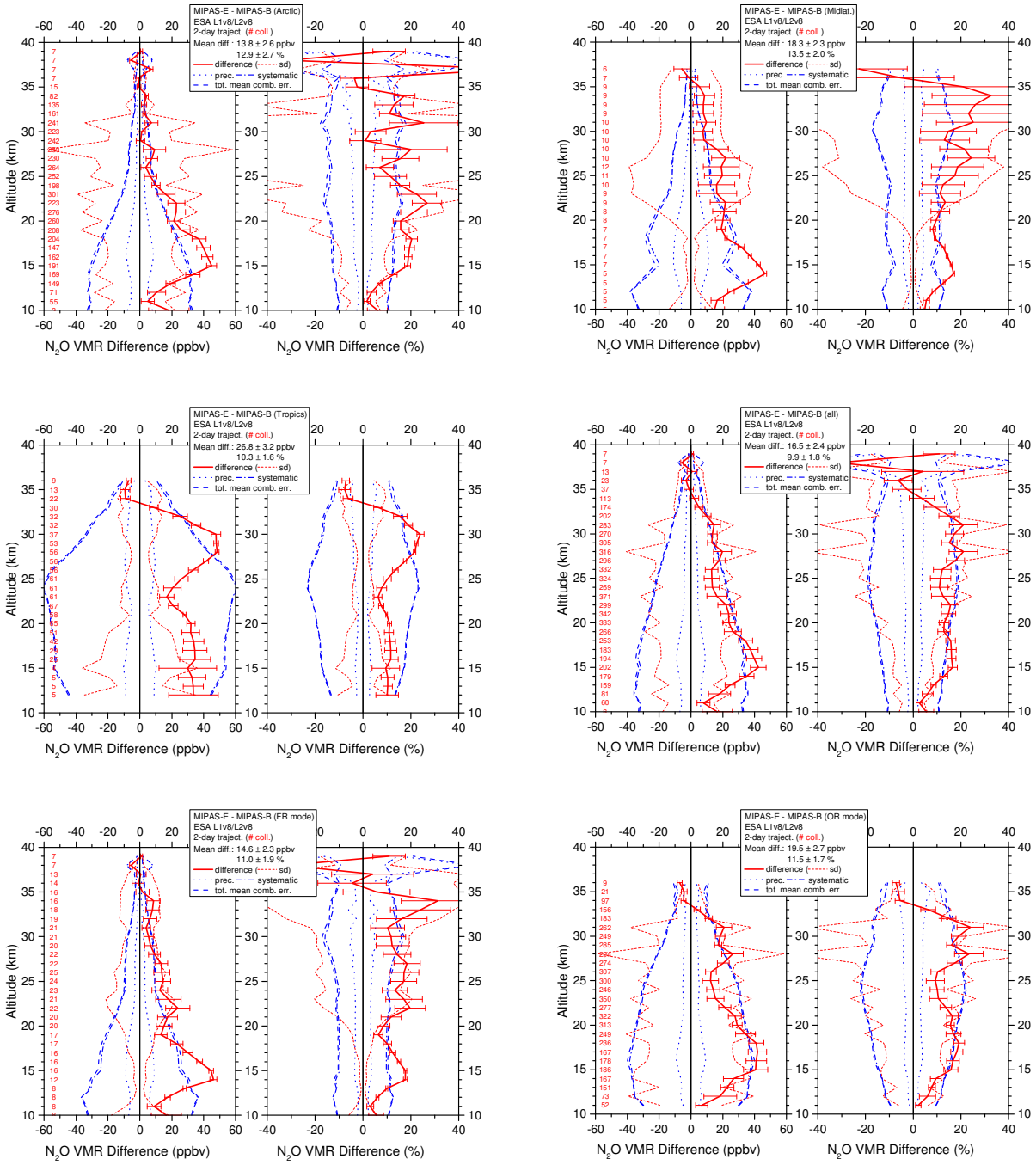

Figure 7. Same as Figure 3 but for N_2O.

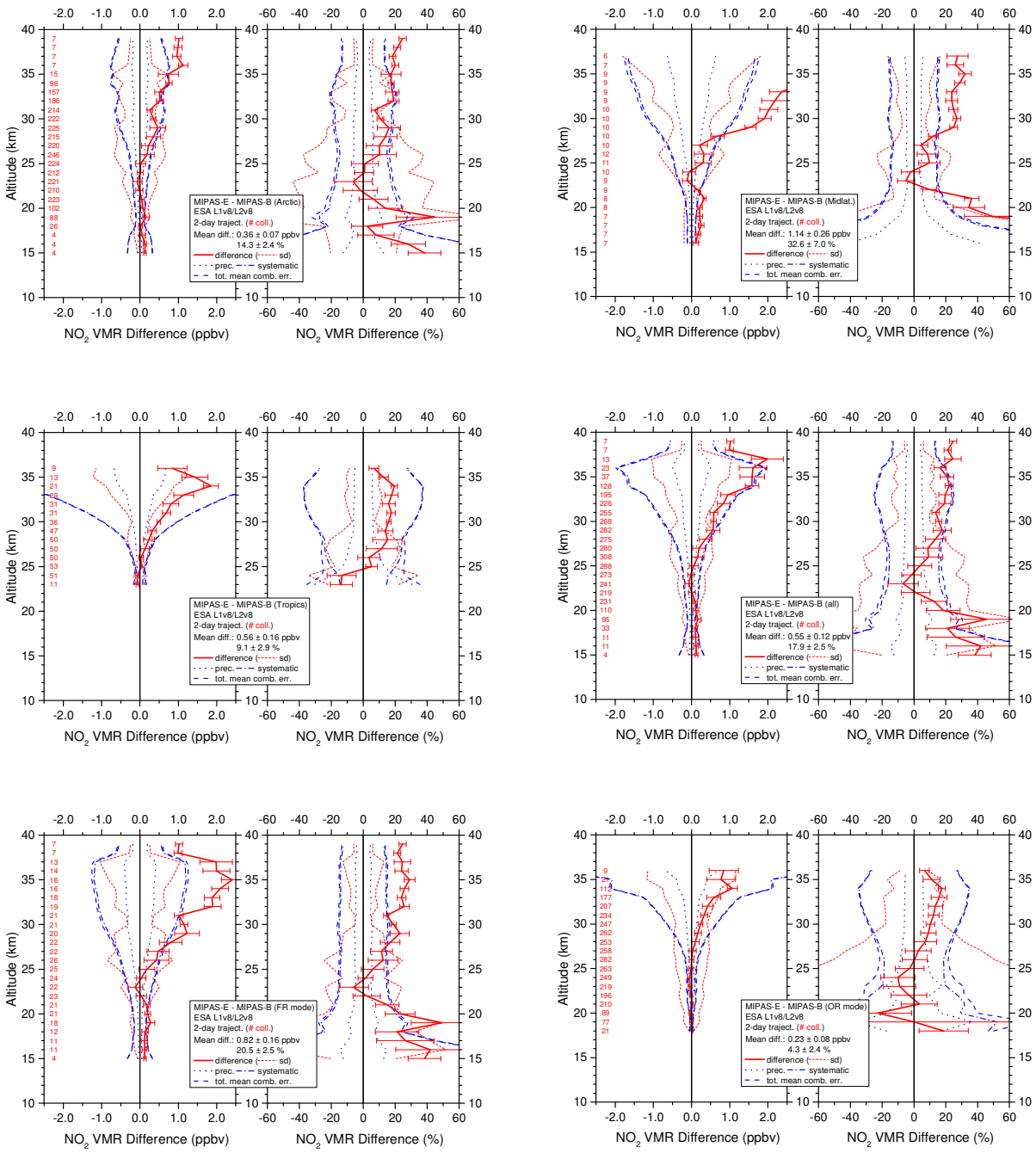

Figure 8. Same as Figure 3 but for NO_2.

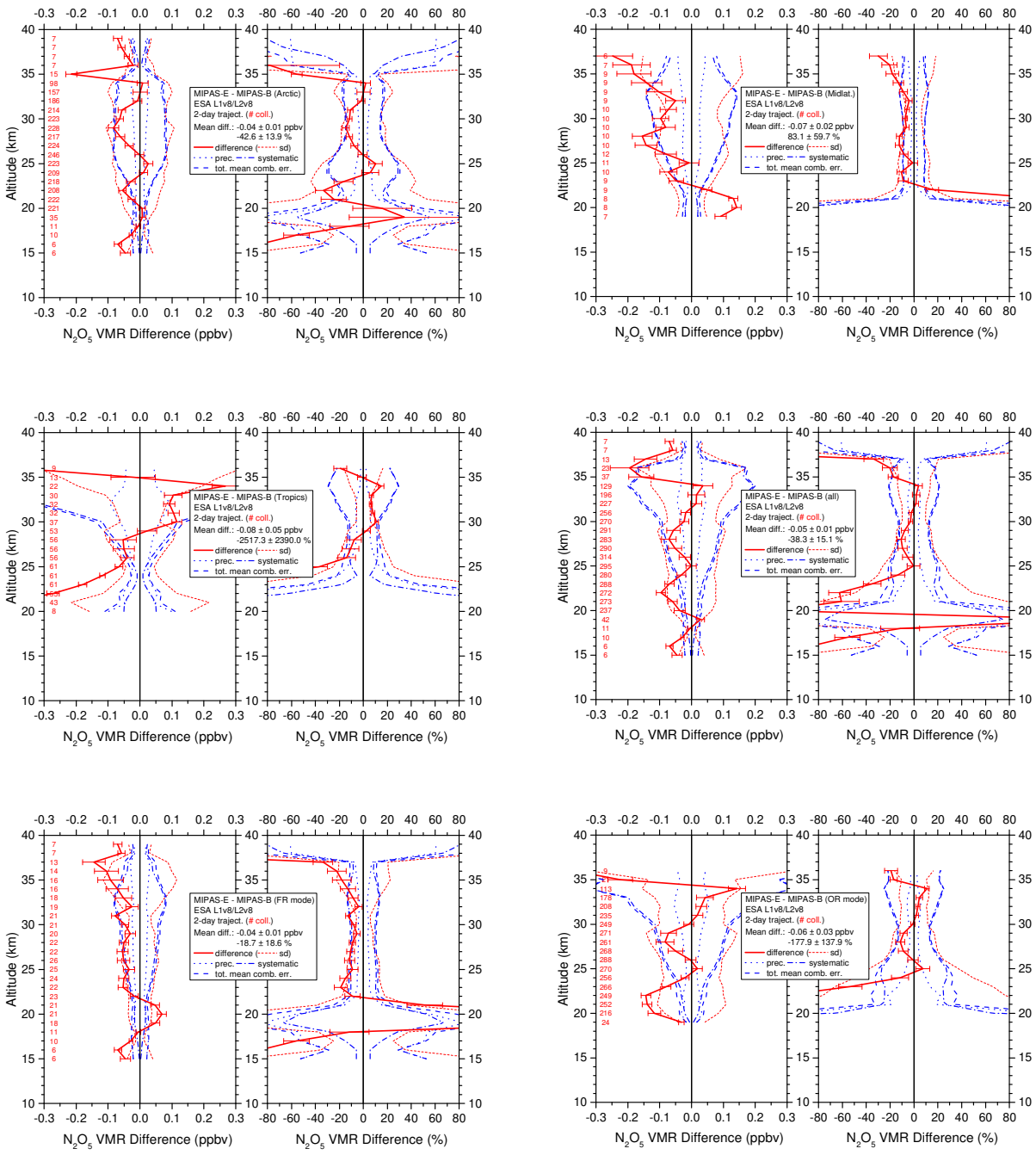

Figure 9. Same as Figure 3 but for N_2O_5.

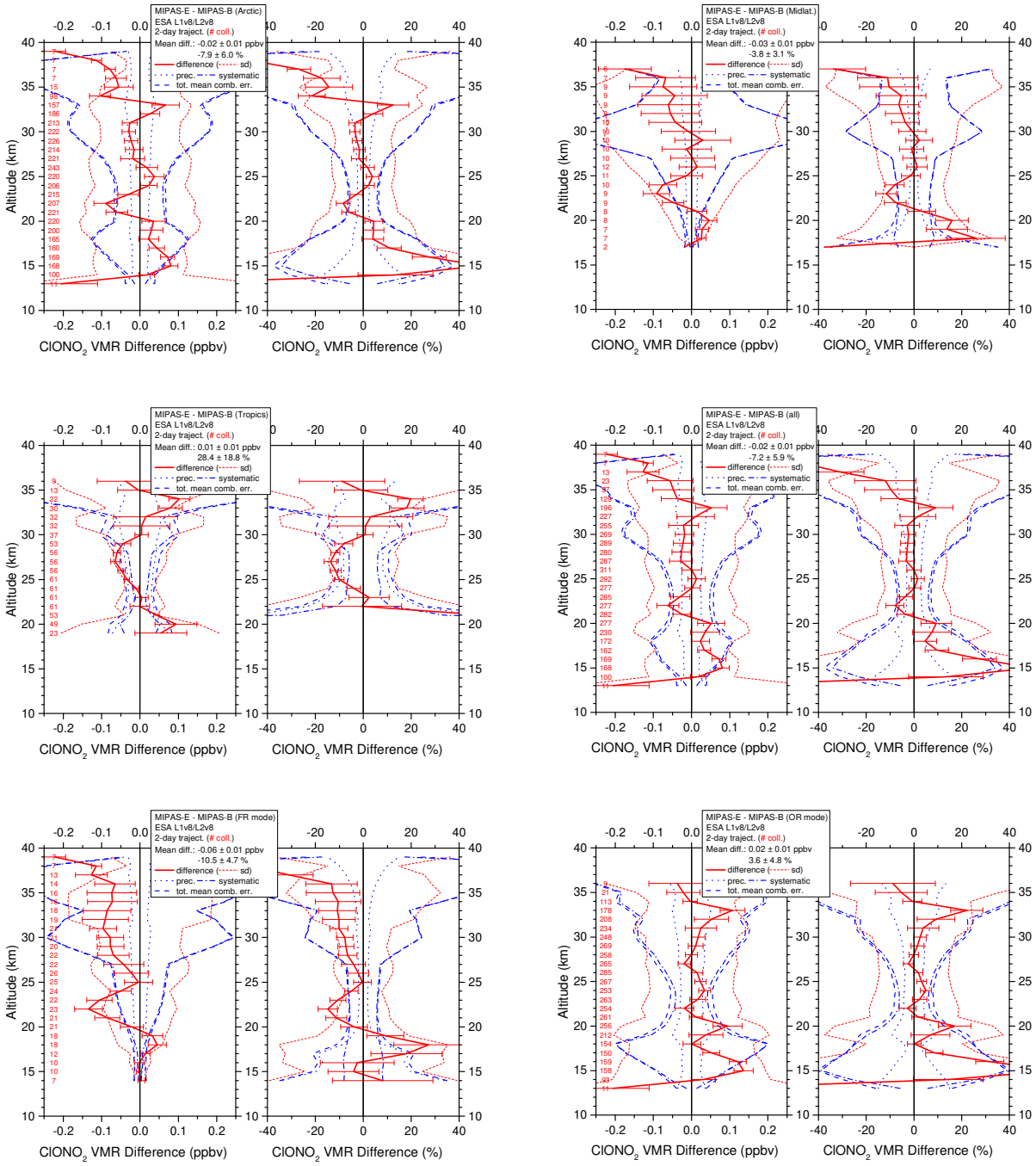

Figure 10. Same as Figure 3 but for $ClONO_2$.

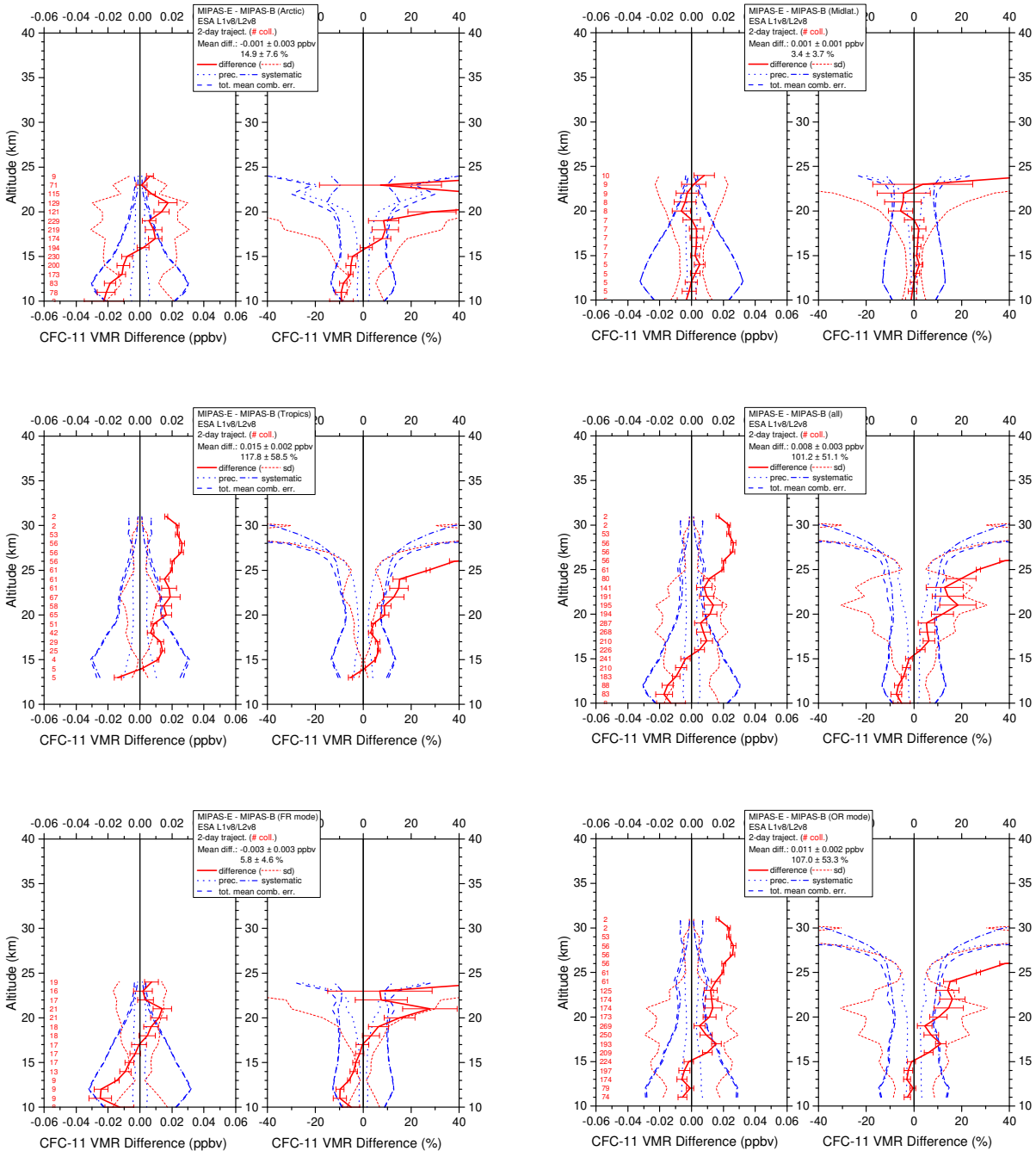

Figure 11. Same as Figure 3 but for CFC-11.

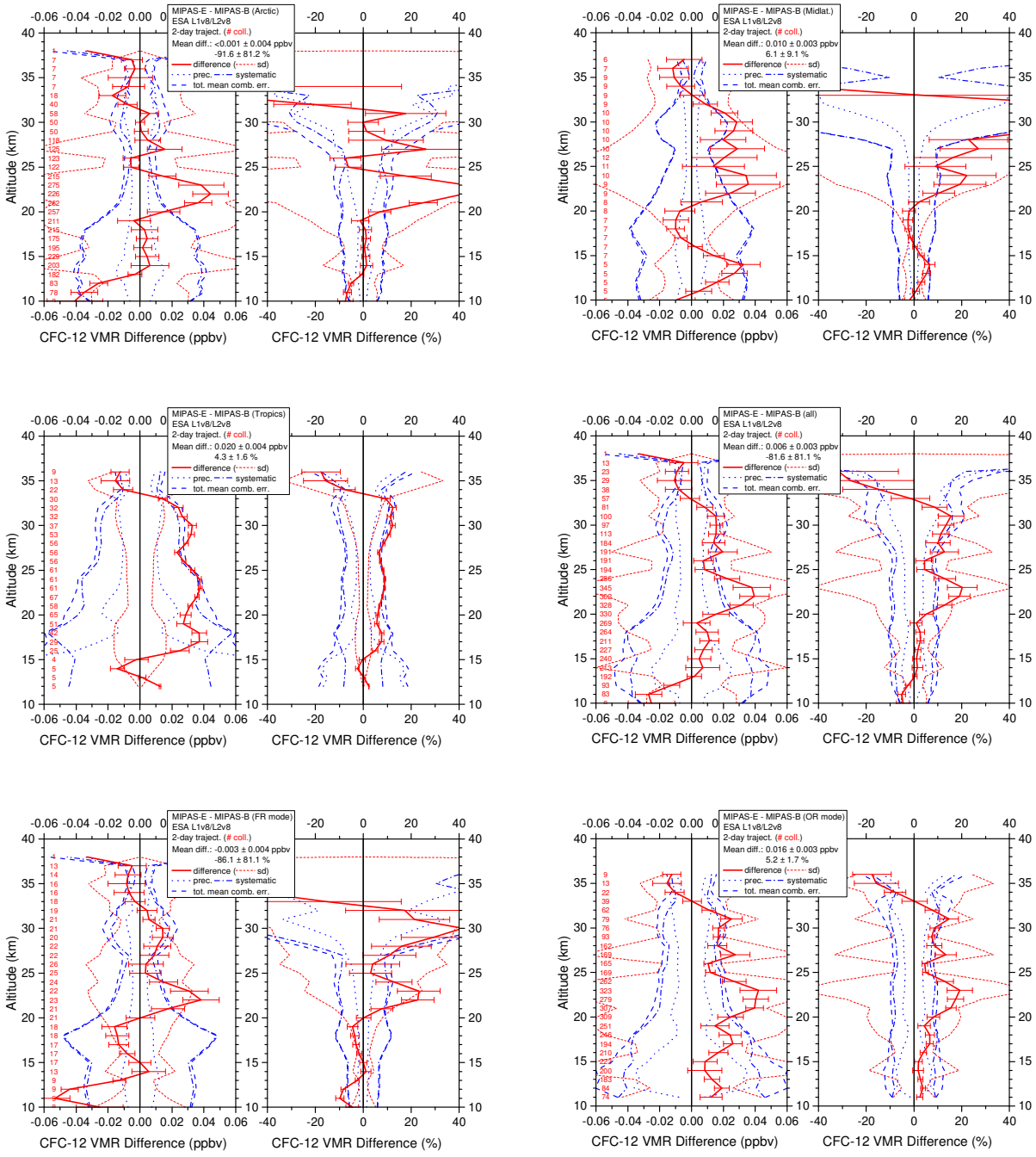

Figure 12. Same as Figure 3 but for CFC-12.

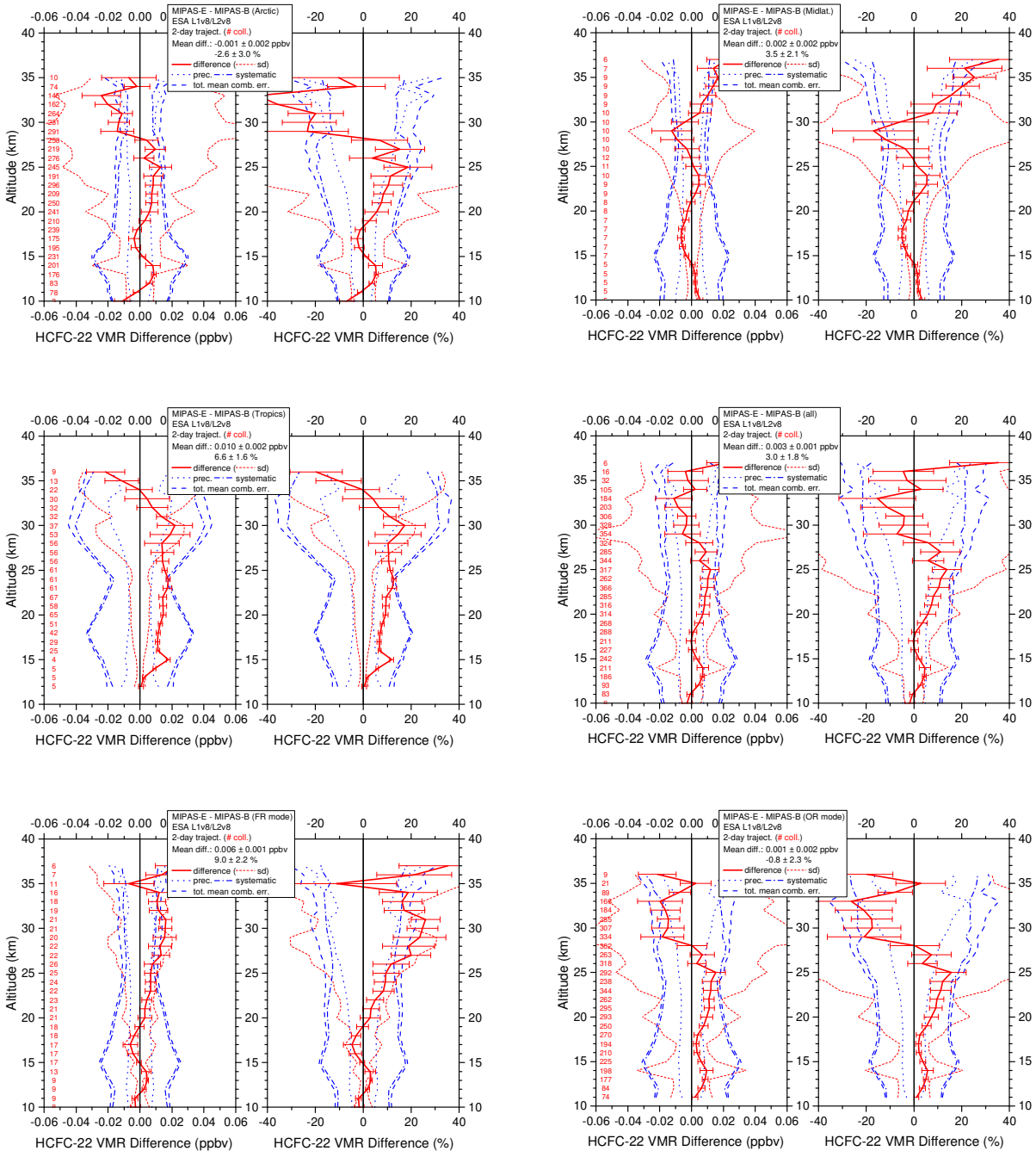

Figure 13. Same as Figure 3 but for HCFC-22.

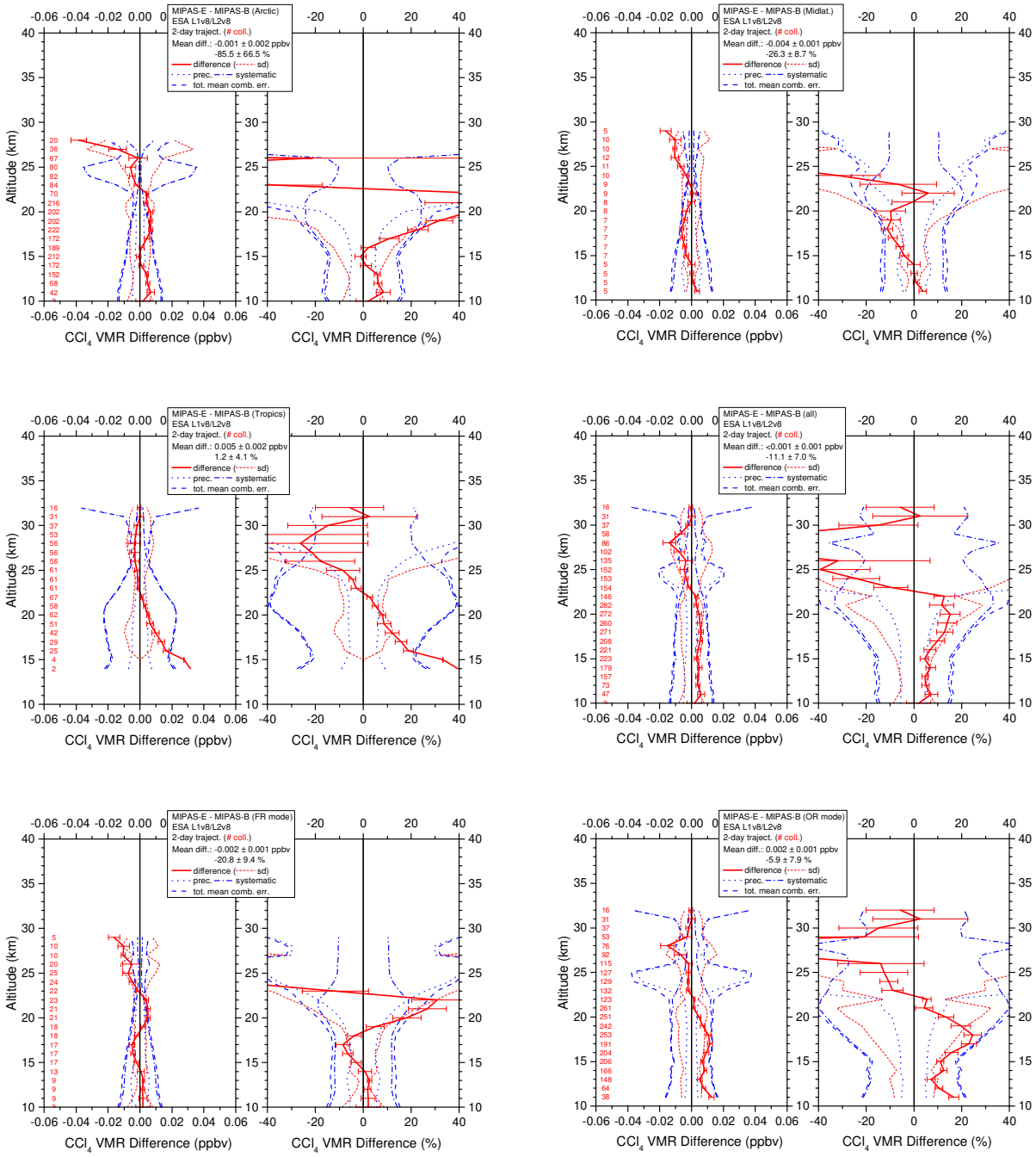

Figure 14. Same as Figure 3 but for CCl_4.

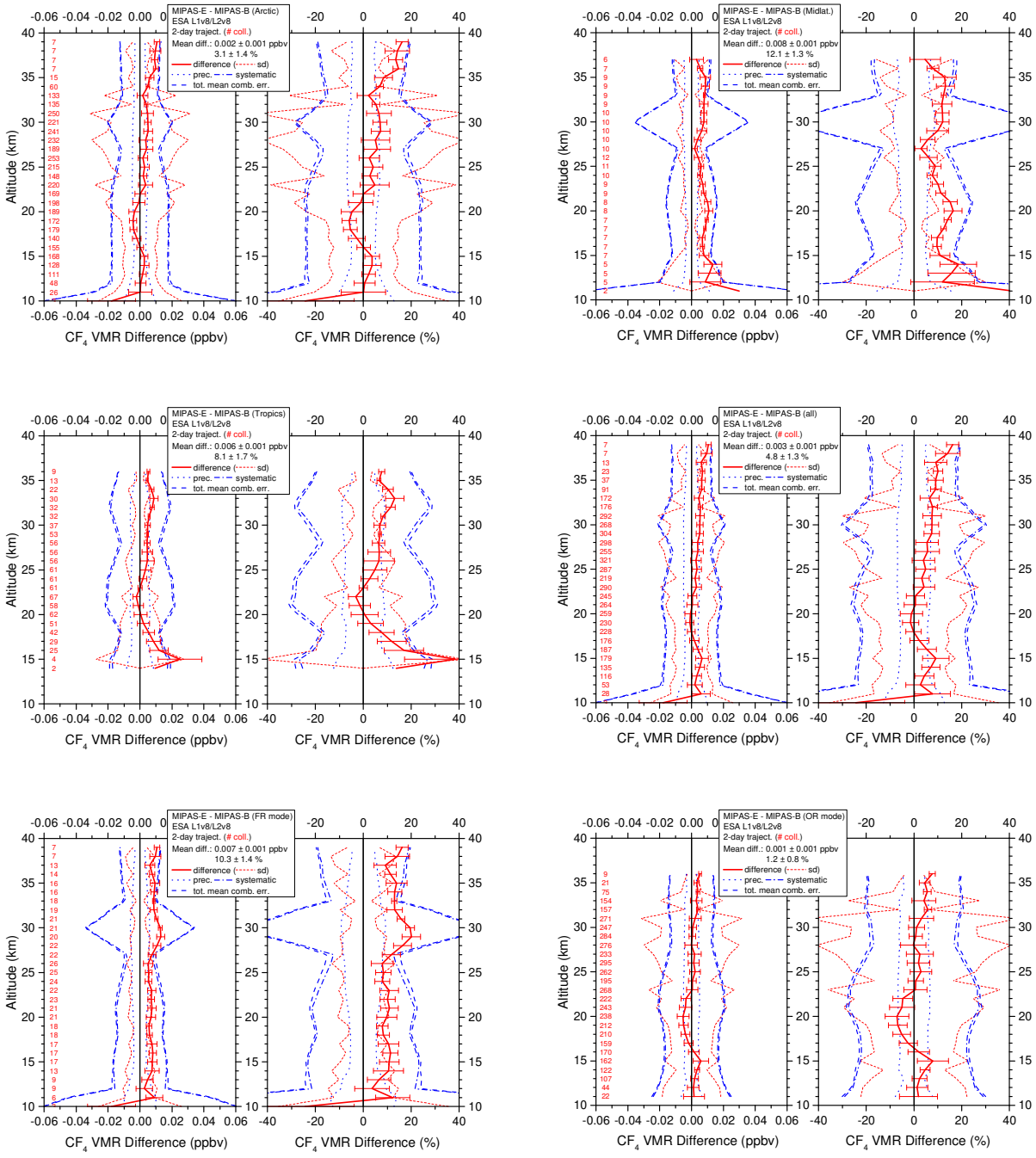

Figure 15. Same as Figure 3 but for CF_4.

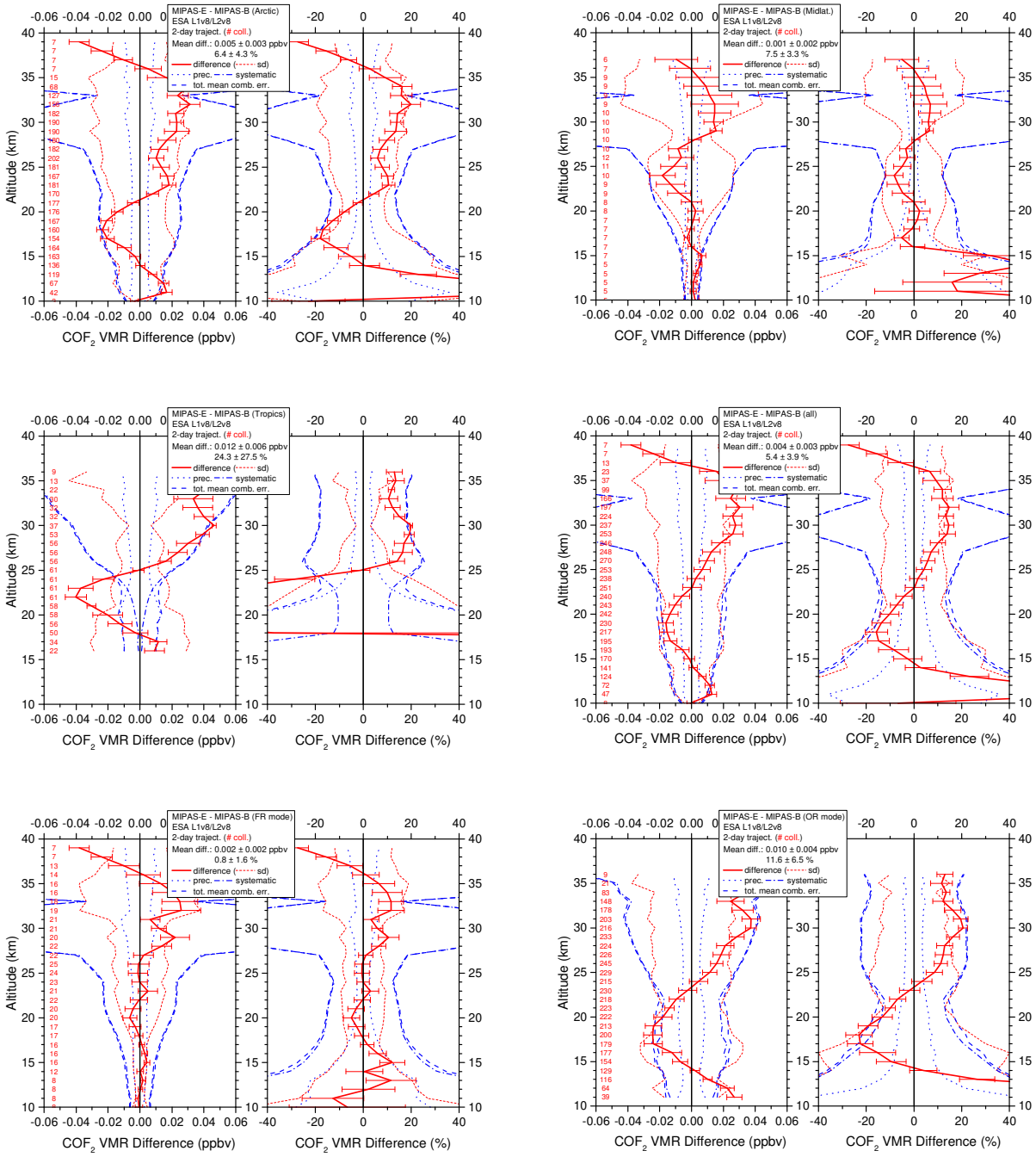

Figure 16. Same as Figure 3 but for COF_2.

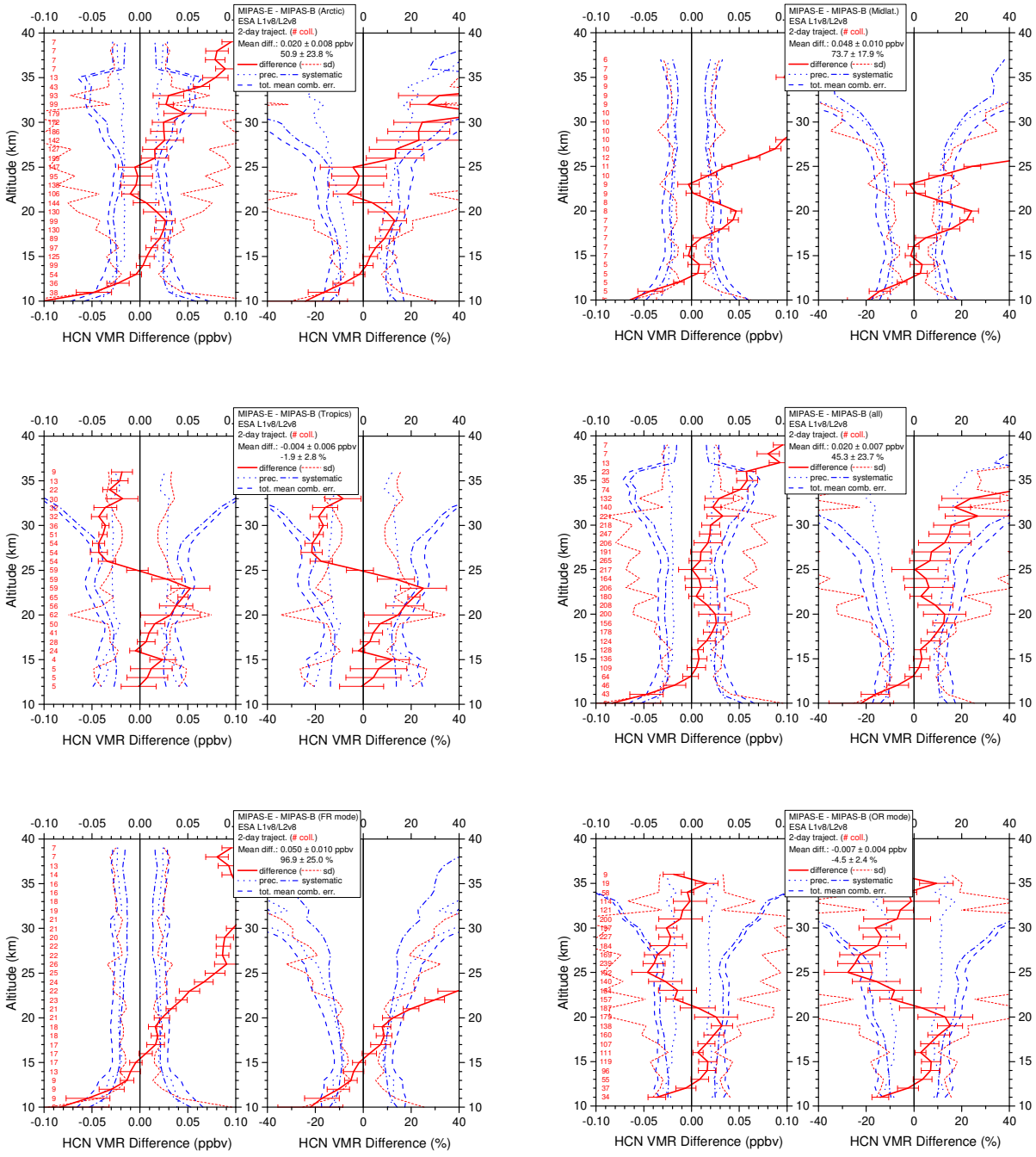

Figure 17. Same as Figure 3 but for HCN.

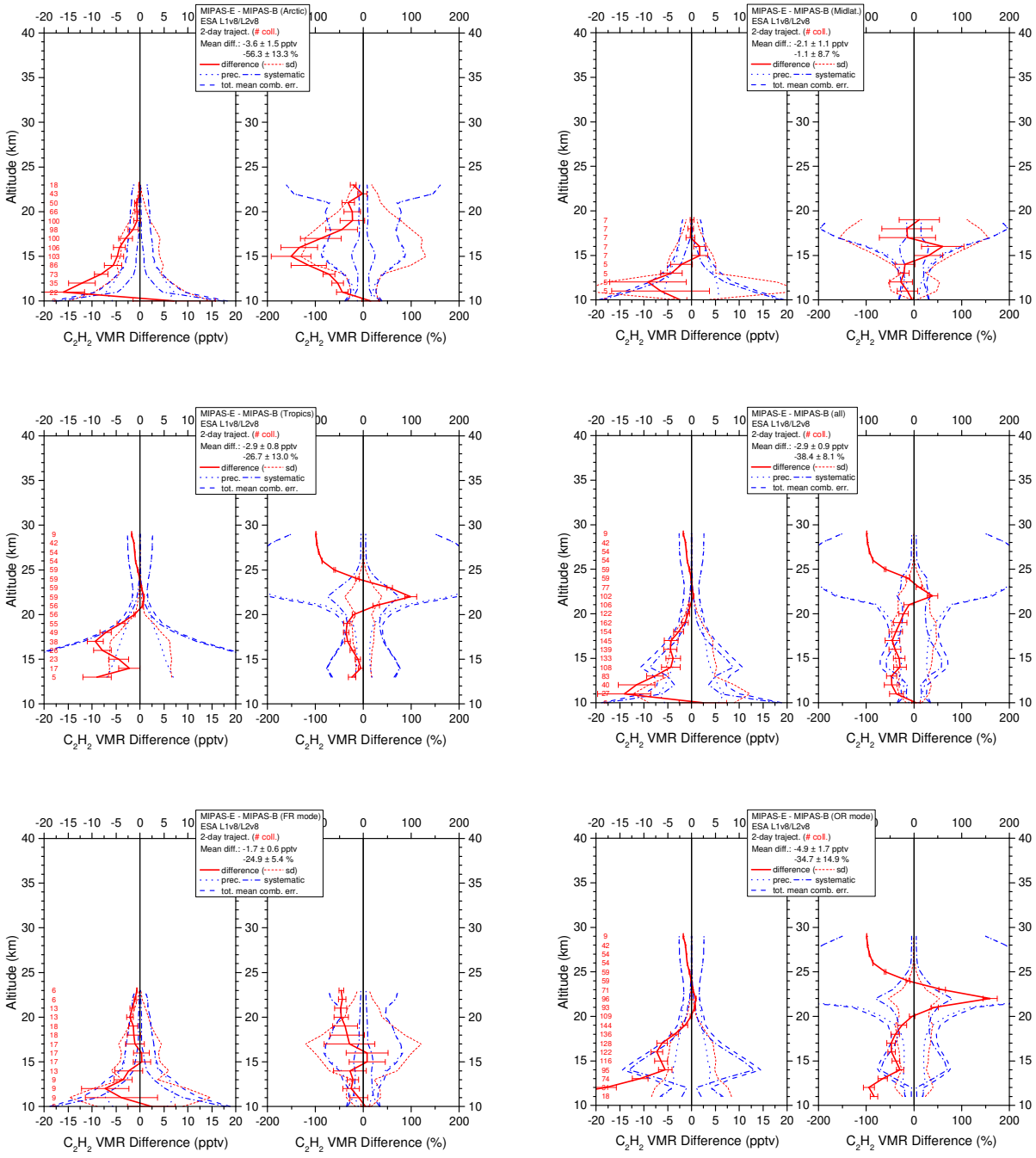

Figure 18. Same as Figure 3 but for C_2H_2.

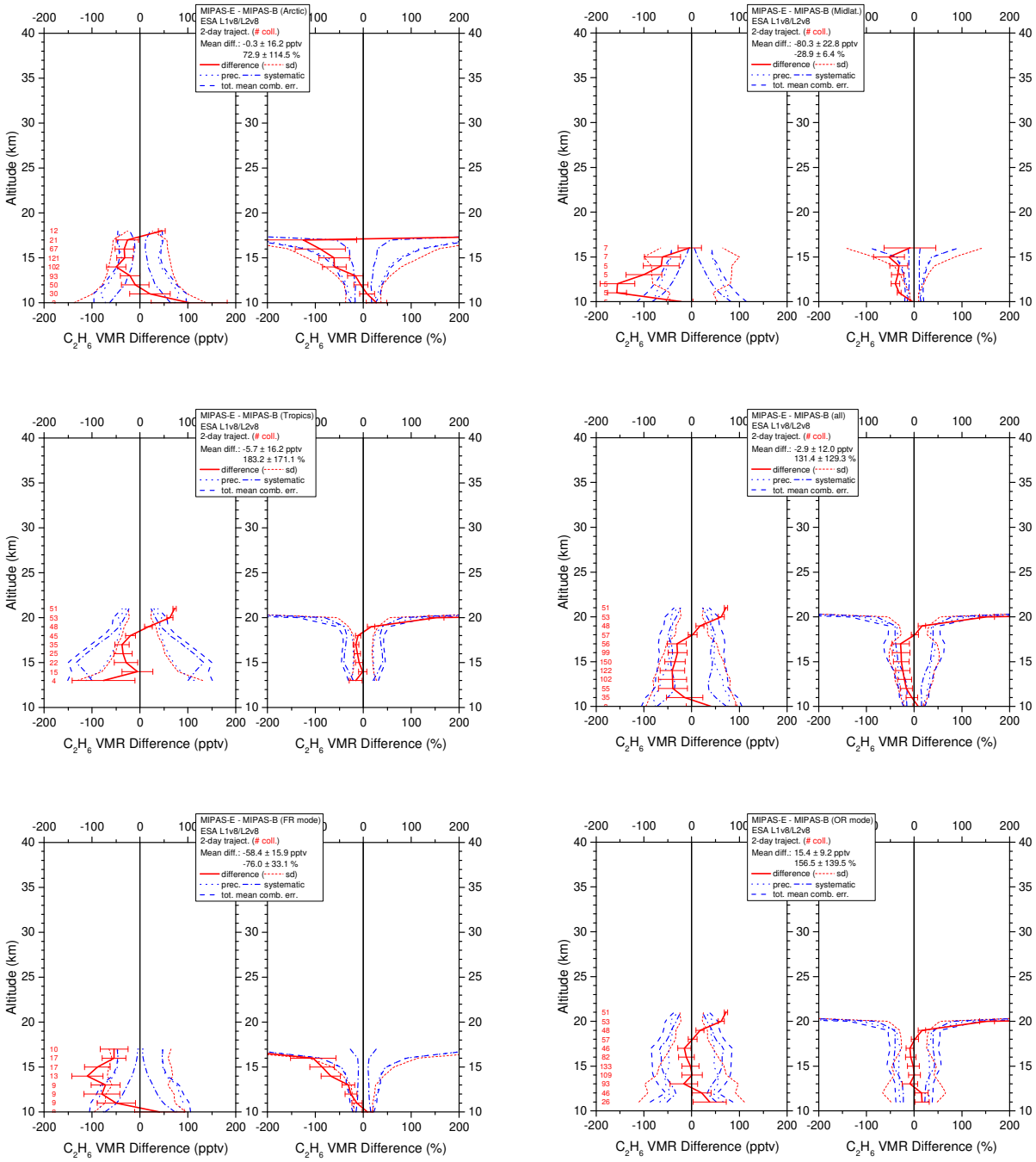

Figure 19. Same as Figure 3 but for C_2H_6.

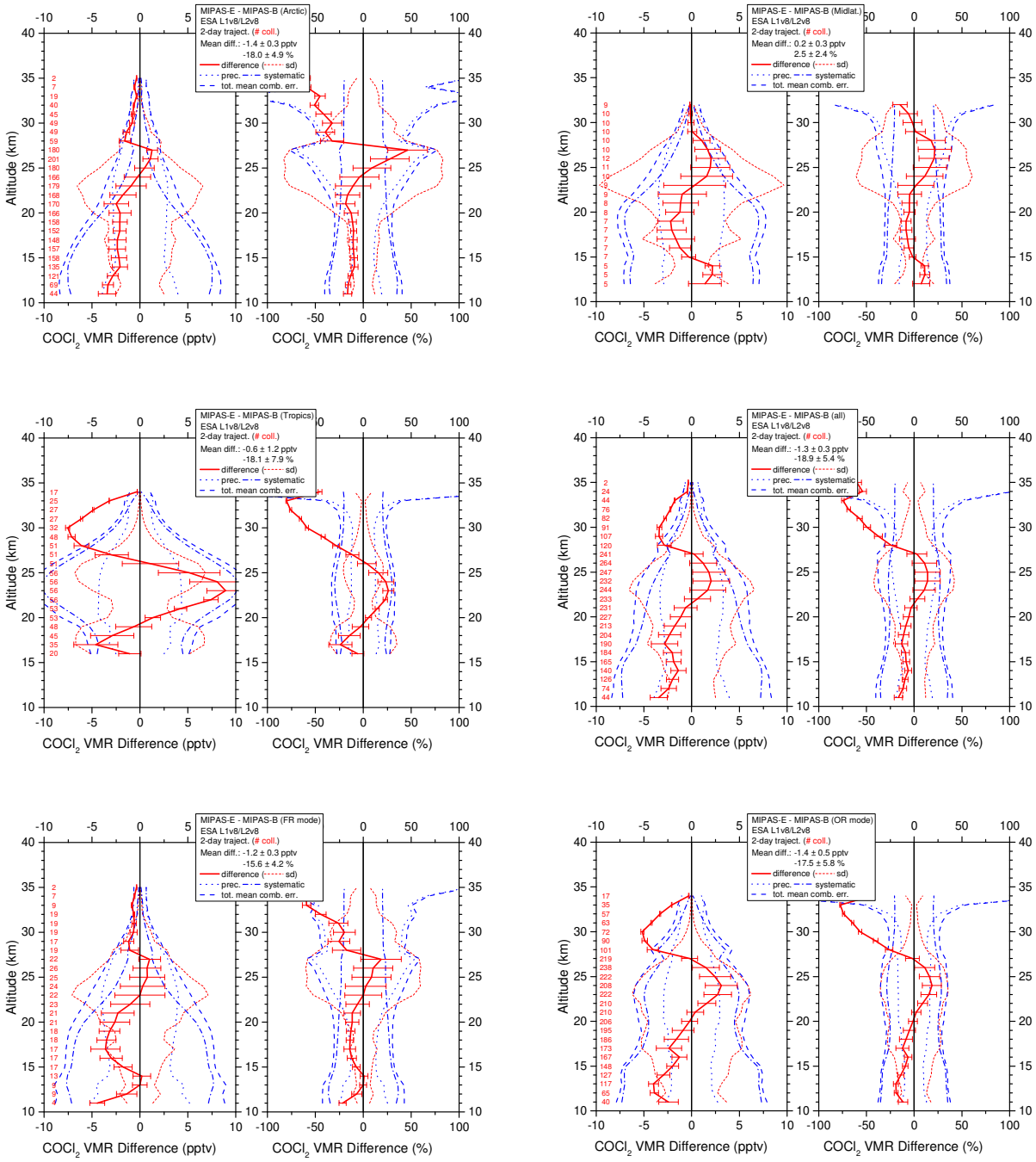

Figure 20. Same as Figure 3 but for $COCl_2$.

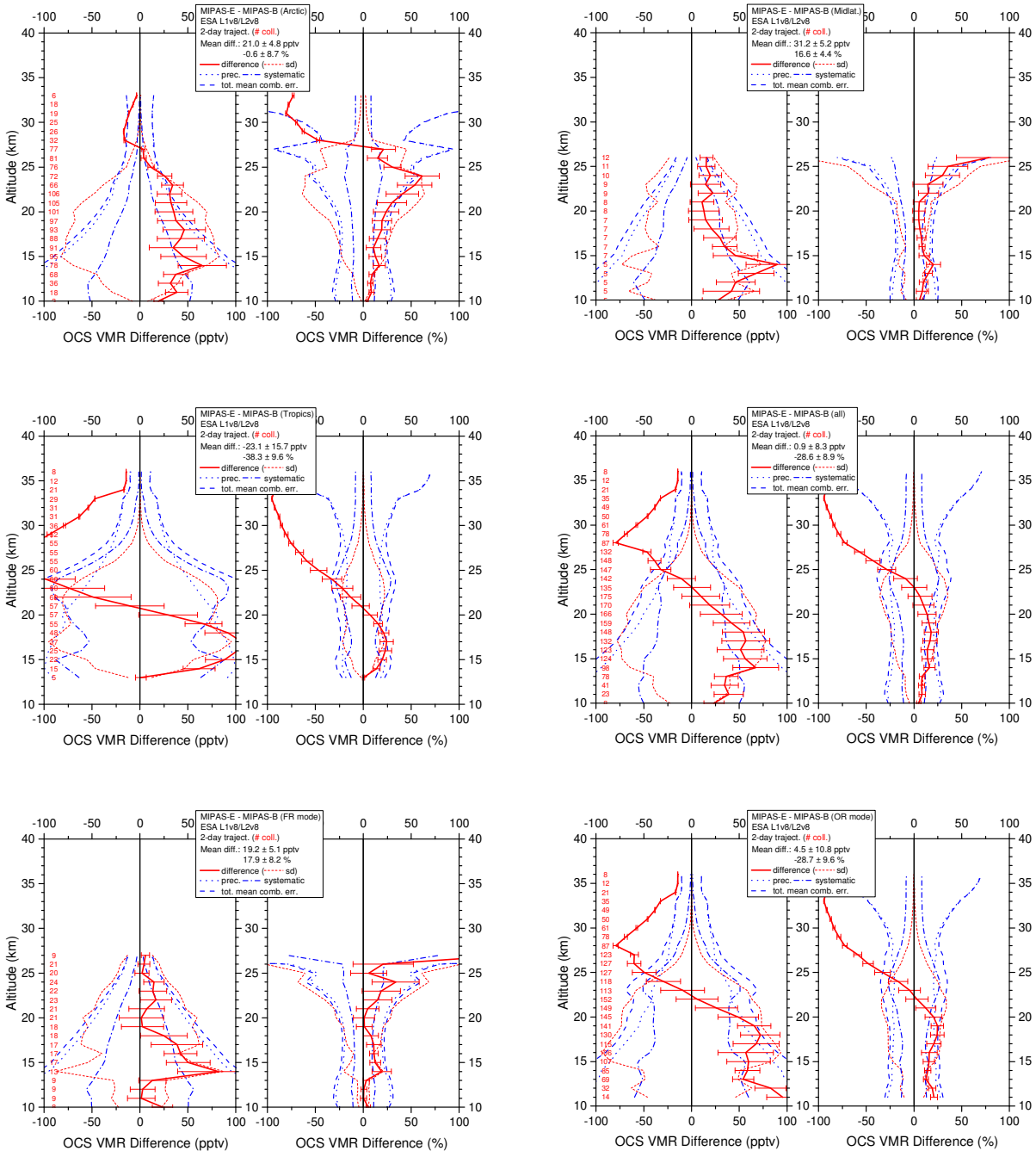

Figure 21. Same as Figure 3 but for OCS.

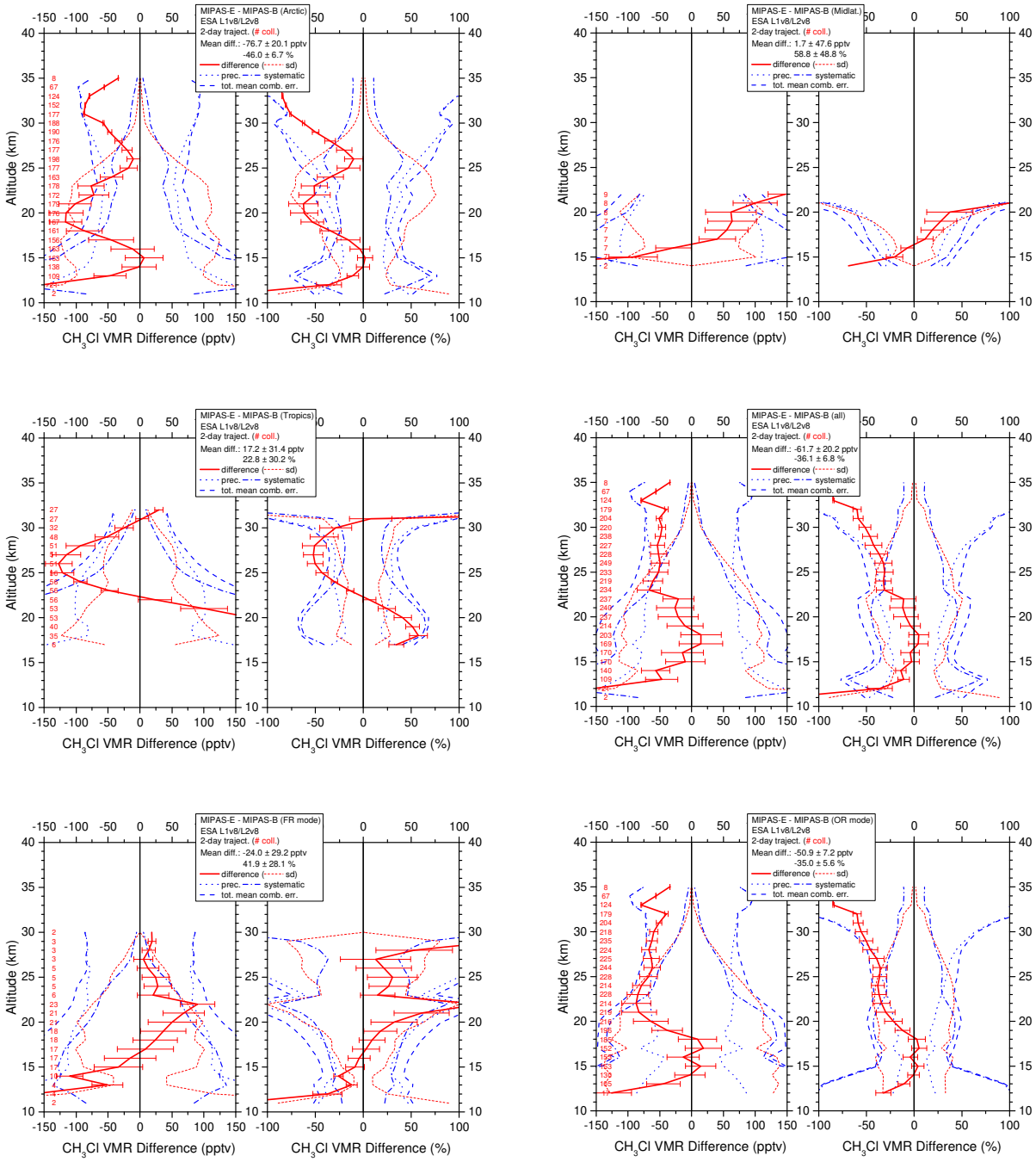

Figure 22. Same as Figure 3 but for CH_3Cl.